JOURNAL OF AIRCRAFT
Vol. 46, No. 6, November–December 2009

Guidance, Navigation, and Control System Design for Tripropeller Vertical-Takeoff-and-Landing Unmanned Air Vehicle

Rui Huang,* Yong Liu,* and J. Jim Zhu†
Ohio University, Athens, Ohio 45701

DOI: 10.2514/1.34476

In this paper, we present the design and development of the guidance, navigation, and control system of a small vertical-takeoff-and-landing unmanned air vehicle based on a 6 degrees-of-freedom nonlinear dynamic model. The vertical-takeoff-and-landing unmanned air vehicle is equipped with three propellers for vertical thrust, and thrust differential together with a set of yaw trim flaps are used for 3 degrees-of-freedom attitude and thrust control actuation. The focus is on the 6 degrees-of-freedom flight control algorithm design using the trajectory linearization control method, along with simulation verification and robustness tests. Hardware and software implementation of the flight controller and onboard navigation sensors are also briefly discussed.

Nomenclature

$A_{i\cdot k}$	=	state matrix representing desired closed-loop dynamics, diag($[-\alpha_{ijk}]$)
C_{D_V}	=	drag force coefficient, N · s^2/m^2
D	=	drag force, N
F	=	total longitudinal, lateral, and normal force in the body-fixed frame, $[F_x \quad F_y \quad F_z]^T$, N
F_{com}	=	command for longitudinal, lateral, and normal force in the body-fixed frame, $[F_{x_{\text{com}}} \quad F_{y_{\text{com}}} \quad F_{z_{\text{com}}}]^T$, N
F_{ctrl}	=	control force correction in the body-fixed frame, calculated by guidance inner-loop feedback, $[F_{x_{\text{ctrl}}} \quad F_{y_{\text{ctrl}}} \quad F_{z_{\text{ctrl}}}]^T$, N
F_{nom}	=	nominal longitudinal, lateral, and normal force in the body-fixed frame, calculated by guidance inner-loop pseudoinverse, $[F_{x_{\text{nom}}} \quad F_{y_{\text{nom}}} \quad F_{z_{\text{nom}}}]^T$, N
f	=	longitudinal, lateral, and normal control force in the body-fixed frame, produced by the thrust of the three propellers, $[f_x \quad f_y \quad f_z]^T$, N
$f_{z_{\text{com}}}$	=	commanded total thrust force in body z direction, N
g	=	gravity constant, 9.81
I^p_{pq}, I^p_{qr}, I^q_{pp}, I^q_{rr}, I^r_{pq}, I^r_{qr}, g^p_l, g^p_n, g^q_m, g^r_l, g^r_n	=	inertial constants
K_{I_i}	=	3×3 matrix, integral feedback gain ($i = 1$, guidance outer-loop/position control; $i = 2$, guidance inner-loop/body velocity control; $i = 3$, attitude control outer-loop/Euler angle control; $i = 4$, attitude control inner-loop/body rate control)
K_{P_i}	=	3×3 matrix, proportional feedback gain
M	=	total moment about the x, y, and z axis of the body-fixed frame (roll, pitch, and yaw, respectively), $[M_x \quad M_y \quad M_z]^T$, Nm
M_{com}	=	command of moment about the x, y, and z axis, $[M_{x_{\text{com}}} \quad M_{y_{\text{com}}} \quad M_{z_{\text{com}}}]^T$, Nm
M_{ctrl}	=	correction of moment about the x, y, and z axis, calculated by attitude inner-loop feedback, $[M_{x_{\text{ctrl}}} \quad M_{y_{\text{ctrl}}} \quad M_{z_{\text{ctrl}}}]^T$, Nm
M_{nom}	=	nominal moment about the x, y, and z axis, calculated by attitude inner-loop pseudoinverse, $[M_{x_{\text{nom}}} \quad M_{y_{\text{nom}}} \quad M_{z_{\text{nom}}}]^T$, Nm
m	=	mass, kg
P	=	position of aircraft, in earth-fixed frame, $[X \quad Y \quad Z]^T$, m
P_{com}	=	position trajectory command to the aircraft, in the earth-fixed frame, $[X_{\text{com}} \quad Y_{\text{com}} \quad Z_{\text{com}}]^T$, m
P_{err}	=	position tracking error, in the earth-fixed frame, $[X_{\text{err}} \quad Y_{\text{err}} \quad Z_{\text{err}}]^T$, m
P_{nom}	=	nominal position trajectory in the earth-fixed frame, $[X_{\text{nom}} \quad Y_{\text{nom}} \quad Z_{\text{nom}}]^T$, m
P_{sen}	=	sensed position of aircraft, in the earth-fixed frame, measured by inertial navigation system/Global Positioning System, $[X_{\text{sen}} \quad Y_{\text{sen}} \quad Z_{\text{sen}}]^T$, m
U	=	control effectors; $[U_{1_{\text{com}}} \quad U_{2_{\text{com}}} \quad U_{3_{\text{com}}} \quad U_{4_{\text{com}}}]^T$, U_{1_com}, U_{2_com}, U_{3_com} (voltage applied to the front, back left, and back right motors, respectively), V; U_{4_com} (yaw flap deflection angle), deg
U_{com}	=	attitude control effector command generated by the attitude inner-loop control allocation; $[U_{1_{\text{com}}} \quad U_{2_{\text{com}}} \quad U_{3_{\text{com}}} \quad U_{4_{\text{com}}}]^T$, U_{1_com}, U_{2_com}, U_{3_com}, U_{4_com}, deg
V	=	longitudinal, lateral, and normal body velocity along the x, y, z directions, in the body-fixed frame, $[u \quad v \quad w]^T$
V_{com}	=	commanded body velocity, input to the guidance inner loop, $[u_{\text{com}} \quad v_{\text{com}} \quad w_{\text{com}}]^T$, m/s
V_{ctrl}	=	body velocity correction, calculated by guidance outer-loop feedback, $[u_{\text{ctrl}} \quad v_{\text{ctrl}} \quad w_{\text{ctrl}}]^T$, m/s

Presented as Paper 6459 at the AIAA Guidance, Navigation and Control Conference and Exhibit, Hilton Head, South Carolina, 20–23 August 2007; received 7 September 2007; revision received 8 October 2008; accepted for publication 17 October 2008.

*School of Electrical Engineering and Computer Science.
†Professor, the School of Electrical Engineering and Computer Science. Senior Member AIAA.

V_{err} = tracking error of body velocity, $[\,u_{\text{err}} \quad v_{\text{err}} \quad w_{\text{err}}\,]^T$, m/s
V_{nom} = nominal body velocity, calculated by guidance outer-loop pseudoinverse, $[\,u_{\text{nom}} \quad v_{\text{nom}} \quad w_{\text{nom}}\,]^T$, m/s
V_{sen} = sensed longitudinal, lateral, and normal body velocity along the x, y, z directions, in the body-fixed frame, measured by inertial navigation system, $[\,u_{\text{sen}} \quad v_{\text{sen}} \quad w_{\text{sen}}\,]^T$, m/s
α_{ijk} = controller parameters; where i is defined as in K_{Pi} and K_{Ii}; $j = 1, 2, 3$, which represents roll, pitch, and yaw channels, respectively; $k = 1, 2$, as defined in Eq. (10)
γ = roll, pitch, and yaw Euler angle (defined by yaw-pitch-roll sequence of rotation) trajectory of the vehicle, $[\,\phi \quad \theta \quad \psi\,]^T$, rad
γ_{com} = roll, pitch, and yaw Euler angle command to attitude outer loop, $[\,\phi_{\text{com}} \quad \theta_{\text{com}} \quad \psi_{\text{com}}\,]^T$, rad
γ_{ctrl} = feedback corrective roll, pitch, yaw Euler angle command, $[\,\phi_{\text{ctrl}} \quad \theta_{\text{ctrl}} \quad \psi_{\text{ctrl}}\,]^T$, rad
γ_{err} = tracking error of roll, pitch, yaw Euler angle of aircraft, $[\,\phi_{\text{err}} \quad \theta_{\text{err}} \quad \psi_{\text{err}}\,]^T$
γ_{nom} = nominal roll, pitch, and yaw Euler angle trajectory, $[\,\phi_{\text{nom}} \quad \theta_{\text{nom}} \quad \psi_{\text{nom}}\,]^T$, rad
γ_{sen} = sensed roll, pitch, and yaw Euler angle trajectory measured by inertial navigation system/Global Positioning System, $[\,\phi_{\text{sen}} \quad \theta_{\text{sen}} \quad \psi_{\text{sen}}\,]^T$, rad
ζ = damping ratio
ω = body roll, pitch, yaw rate, in the body-fixed frame, of the vehicle, $[\,p \quad q \quad r\,]^T$, rad/s
ω_{com} = commanded body rate, input to the attitude inner loop, $[\,p_{\text{com}} \quad q_{\text{com}} \quad r_{\text{com}}\,]^T$, rad/s
ω_{ctrl} = body rate correction, calculated by attitude outer-loop feedback, $[\,p_{\text{ctrl}} \quad q_{\text{ctrl}} \quad r_{\text{ctrl}}\,]^T$, rad/s
ω_{err} = tracking error of body roll, pitch, yaw rate, in the body-fixed frame, $[\,p_{\text{err}} \quad q_{\text{err}} \quad r_{\text{err}}\,]^T$, rad/s
ω_{nom} = nominal body rate, calculated by attitude outer-loop feedforward, $[\,p_{\text{nom}} \quad q_{\text{nom}} \quad r_{\text{nom}}\,]^T$, rad/s
ω_{sen} = sensed body roll, pitch, yaw rate, in the body-fixed frame, measured by inertial navigation system, $[\,p_{\text{sen}} \quad q_{\text{sen}} \quad r_{\text{sen}}\,]^T$, rad/s
ω_n = natural frequency, approximate bandwidth

I. Introduction

UNMANNED aerial vehicles (UAVs) have attracted significant attention in recent years for both military and civilian applications. Among the different configurations of UAVs, those UAVs with vertical-takeoff-and-landing (VTOL) and hovering (or near-hovering) flight capabilities are of particular interest. They are ideal platforms for intelligence, surveillance, and reconnaissance, as well as search and rescue. The helicopter and tilt-rotor aircraft, such as the V-22 Osprey, are two typical VTOL aircraft with the hovering capability. However, they both employ complex rotor mechanisms to achieve these capabilities. For small VTOL aircraft, such as a small UAV equipped with multiple propulsion units, it is possible to use differential thrust as attitude control effectors, due to the small inertia of the rotors. In this paper, the guidance, navigation, and control (GNC) system design for a tripropeller UAV is introduced, based on a 6 degree-of-freedom (6DOF) nonlinear dynamic model.

The structure of the tripropeller UAV is shown in Fig. 1a, herein referred to as the Ohio University UFO (unique flying object) or OU UFO, which is based on a flight control research and education test bed developed by Quanser, Inc.[‡] known as the Quanser UFO (see Fig. 1b). Both of them are installed with three propellers, which are driven by dc motors. The attitude control of the UFOs is achieved by differential thrust of the propellers. The difference between the OU UFO and the Quanser UFO is that the latter has only 3DOF rotational motion, with attitude angles measured by three optical encoders mounted on the gimbal axes; whereas, the former is capable of 6DOF flight, with an additional 2DOF of control actuation provided by the flaps mounted in the slipstream of the propellers, and the attitude and position of the vehicle measured by an onboard inertial navigation system and Global Positioning System (GPS). The flaps produce a net yaw moment when the front and rear flaps are actuated differentially and produce a side force when they are actuated collectively. The key physical, geometrical, and operational properties of the Delta-UFO are summarized in Table 1. It is noted that the design was not optimized, and the expected performance can be improved significantly by optimally matching the motor and propeller.

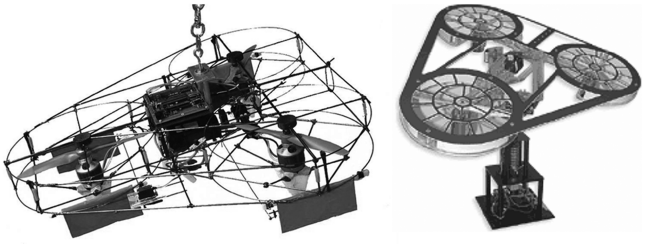

a) Ohio University UFO b) Quanser UFO

Fig. 1 Tripropeller VTOL UAV.

The trirotor configuration for VTOL vehicles has been explored before, such as NASA Langley Research Center's VTOL-cruising aircraft concept model [1] shown in Fig. 2a and the Sky Commuter concept vehicle prototype[§] shown in Fig. 2b, developed by Flight Innovations, Inc. (originally designed by Fred Barker, a Boeing engineer, intended as a dual-mode personal transportation vehicle). Recent developments include the University of Adelaide's tilt-prop UAV [2] shown in Fig. 2c and the Affiliated Research Laboratories (UMR), National Center for Scientific Research (CNRS) triprop UAV [3,4], shown in Fig. 2d. Similar vehicles with four propellers have been developed by many researchers, and a noninclusive sample of the "quad-prop" vehicles can be found in [5–14].[¶] Compared to the quad-prop configuration, the triprop configuration reduces the number of propulsion units by one, thereby reducing the complexity and cost, and increasing the reliability of the vehicle. The triprop configuration also has the desirable delta-shaped fuselage profile, as seen in Figs. 2a and 2b. However, the triprop configuration poses a much greater challenge to the flight control system.

Because of its relatively simple mechanical configuration, the key to successful flight of these fixed-pitch, multiprop vehicles is the flight control system. The vehicle dynamics are highly coupled and nonlinear. Moreover, for tracking maneuvering trajectories, the tracking error dynamics are time varying. The controller design is further challenged by the relatively slow actuator dynamics. In the symmetric four-propeller configuration, the reactive yawing moment generated by the propellers is largely decoupled from the pitching and rolling moments, which nominally simplifies the attitude control [5]; whereas, in the asymmetric tripropeller configuration, the yawing moment is coupled with the pitching and rolling moments.

The modeling and control design for quad-prop VTOL UAV structures were developed in [5–14].[¶] In [11,12], a quasi-stationary (hover or near-hover) dynamic model was presented for a four-propeller

[‡]Data available at www.quanser.com.

[§]Information provided for the auction of the Sky Commuter concept vehicle prototype, 2008, http://cgi.ebay.com/ebaymotors/The-last-Concept-Sky-Commuter-aircraft-in-Existence_W0QQcmdZViewItemQQcategoryZ26428QQihZ012QQitemZ220188946461QQrdZ1QQsspagenameZWDVW.

[¶]The Yu-Jing-Ling VTOL UAV of the Nanjing University of Aeronautics and Astronautics, news release and photographs available at http://newsweb.nuaa.edu.cn/nhrw/20138075.htm, http://news.xinhuanet.com/ photo/2007-07/08/content_6343251.htm.

Table 1 Design specifications for the Delta-UFO

Properties	Specifications	Remarks
Gross takeoff weight	5.0 kg (11 lb)	
Vehicle weight	3.5 kg (7.7 lb)	
Nominal payload capability	1.5 kg (3.3 lb)	Can be traded for extra battery
Dimension, $L \times S \times H$	$0.66 \times 0.66 \times 0.15$ m ($26 \times 26 \times 6$ in.)	
Electric motor, max. speed, max. input power	10,000 rpm, 800 W	AXI4120/18 (3)
Propeller, diam × pitch	0.28×0.15 (F), 0.28×0.1 (R) m [11×6 (F), 11×4 (R) in.]	Front propeller is reversed pitch. Static thrust at 10,000 rpm: 4.35 lb per propeller
Nominal battery (voltage, amp-hours, weight)	22.6 V, 6.6 Ah, 1 kg (34 oz)	Lithium polymer rechargeable battery
Flying speed	Est. 20 km/hr (10.8 kt)	Depends on drag and propeller efficiency
Endurance	5 min	Can be extended using small or variable pitch propellers or extra battery
Range	1.67 km (1 mile)	Can be extended using small or variable pitch propellers or extra battery

airframe, known as the X-4 Flyer, including the rotor dynamics and gyroscopic effects. In [13], the dynamic model of the X-4 Flyer was developed including the motor dynamics, aerodynamics, and gyroscopic effects. In [11,13], the velocity and yaw angle controller was developed based on the Lyapunov control function method. In [12], the nonlinear dynamic model was first linearized. A pilot augmentation control system was developed which controls the attitude. A linear proportional feedback control and a linear lead compensator were employed. In [5], an autonomous UAV system based on the X-4 Flyer was introduced, including the UAV hardware, sensor, datalink, onboard computer, ground station, and other components. A simplified linear state-space model was developed. A sliding mode controller was developed for altitude control, and an linear quadratic regulator controller was designed for attitude control. Waslander et al. [14] reported that the altitude control of such UAV was difficult due to the disturbance and model uncertainty.

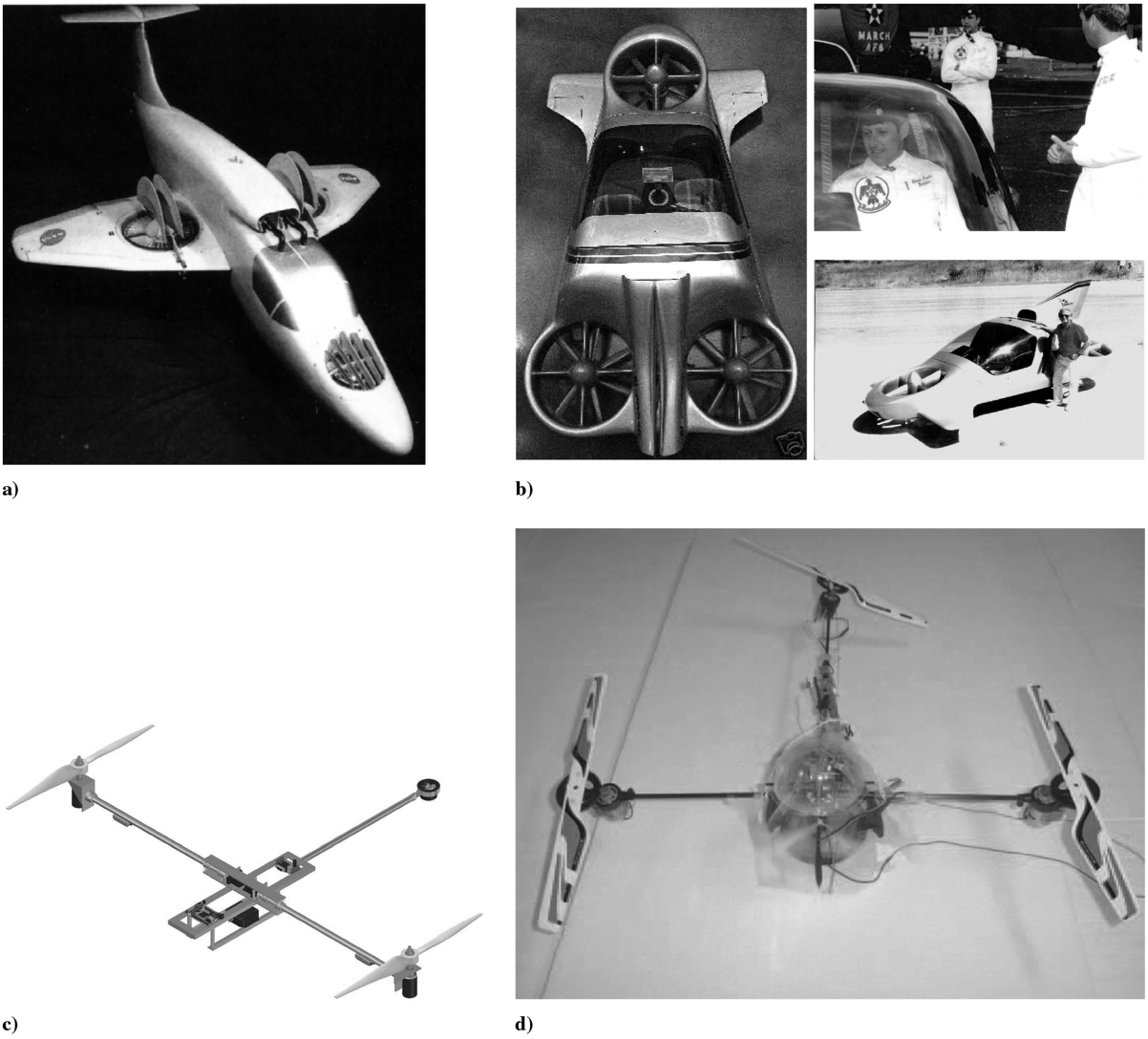

Fig. 2 Trirotor VTOL concept vehicles and prototype UAV models: a) NASA concept vehicle model [1], b) Sky Commuter concept vehicle prototype,[§] c) University of Adelaide tilt-prop UAV [2], and d) UMR CNRS triprop UAV [3,4].

Thus, integral sliding mode control and reinforcement learning were applied to accommodate the disturbance.

The asymmetric structure of tripropeller UAVs makes the attitude control a more challenging problem than the four-propeller counterpart. There does not seem to be a publicly accessible reference about the control system design for the NASA Langley Research Center concept vehicle shown in Fig. 2a (1960s). Since its inception in 1990,[§] some 6 million dollars had been spent on the development of the Sky Commuter concept vehicle prototype without a successful flight. Quoting from available information,[§] "In all its development, this craft has never been more than 10 ft off the ground and ALL the flight tests were crash failures. They had overcome many issues but could not get away from power/rate/control issues. Years of testing. . .. . .never a safe mode flight."

The tilt-prop UAV [2] used a small tail fan to produce pitch control moment, and differential thrust of the main props to produce roll control moment, whereas yaw moment was produced by differentially tilting the main props in the plane of symmetry. The main props were designed to tilt forward 90 deg for fast cruise flight. A classical proportional-integral-derivative (PID) controller and a state-space linear controller were designed for the vehicle based on linearized models. Quoting Prime et al. [2], "The basic PID controller was tested before attempting the more complicated state-space controller. The controller gains for roll and pitch were tuned incrementally after each test run. While liftoff was achieved a number of times, the aircraft could not achieve a stable hover. After a few runs the liftoff characteristics were improving with less severe landings." Further testing was aborted due to a major mechanical failure that severely damaged the test vehicle.

The UMR CNRS triprop UAV [3,4] used the differential thrust to generate roll and pitch control moments and the desired normal thrust. Yaw control moment was produced by tilting the tail rotor laterally, which would generate a side force that was treated by the authors as a disturbance. It is noted that this side force cannot be trimmed by the vehicle control system. However, it is possible to trim it with gravity by rolling the vehicle. However, this will tilt the thrust vector and create a sideslip. Conceivably, the vehicle would not be able to follow a straight path precisely and steadily. Two different types of nonlinear controllers, a nested-saturation controller [3] and a sum-of-saturation-functions controller [4] were developed for the vehicle, and computer simulation results for both controllers were compared in [4]. The simulation scenario was to move from the initial position $[X, Y, Z] = [1, 1, 0]$ m to the final position of $[0, 0, 1]$ and hold there. In both methods, the altitude Z exhibited a 70% overshoot with a settling time of about 10 s, while having an excursion of 20–40 m in the Y direction (depending on the controller gains), and 45–70 m in the X direction with a settling time on the order of 30 to more than 100 s. Hardware-in-loop simulation of the latter controller took some 40 s for the vehicle to rise vertically 0.2 m (about 8 in.), with excursions in the X direction on the order of 0.1 m (about 4 in.), and in Y direction on the order of 0.02 m (about 0.8 in.). Although the controller did achieve stability, noting that the vehicle mass was 0.5 kg, this level of performance is clearly unsatisfactory for real-world applications.

Based on the preceding literature survey of some of the most recent attempts at controlling triprop VTOL configurations, such configurations serve as a challenging test bed for advanced nonlinear control methods. In addition to enabling the advanced vehicle concepts shown in Fig. 2, the control algorithms developed for the tripropeller UAV can be easily adapted to the quad-prop configuration. It may serve as a fault-tolerant controller for the quad-prop UAV; in case one of the four propellers fails, the control system will still be able to maintain stable flight. Thus, the reliability and survivability of the UAV are improved. It should be noted that the thrust-differential controller developed for this type of UAV can also be applied to other aircraft with multiple propulsion units to facilitate fault-tolerant flight control using thrust-differential as secondary control effectors. In the aforementioned VTOL UAV studies, the automatic flight control system is still a pilot augmentation system, in which a pilot is required to observe and close the trajectory tracking loop. To enable autonomous flight, it is necessary that the vehicle be able to follow real-time generated trajectory without pilot intervention.

In this paper, an autonomous 6DOF guidance, navigation, and control system is proposed based on a 6DOF nonlinear dynamic model of the OU UFO. The control structure employs a multiple-loop trajectory linearization controller (TLC). The designed controller is able to follow a feasible guidance trajectory without pilot intervention. Simulation verification of the 6DOF flight of a circular arc trajectory with VTOL is presented. Robustness to disturbances, loop delay, and parametric modeling errors are also tested. The controller not only stabilizes the vehicle, but also tracks the given trajectory autonomously with satisfactory precision and agility for many real-world applications. It is worth noting that this is the first 6DOF flight controller designed using the TLC method. Implementation of the navigation system is also discussed.

The design and simulation testing of the 6DOF controller is an important phase of the ongoing OU UFO project. The development of the project is divided into six phases. The first phase is the modeling and controller design for the 3DOF Quanser UFO. In this phase, the 3DOF Quanser UFO was modeled based on first principles and was implemented in simulation. Then, a TLC attitude controller was designed based on the mathematical model. The controller was integrated with the model in simulation. In the second phase, the 3DOF Quanser UFO was connected to a PC with a data acquisition board. The WinCon software provided by Quanser enabled the real-time hardware-in-the-loop (HIL) test with the control law running on the PC. The results of the first and the second phases were presented in [15–17]. An onboard controller had been developed, tested, and improved in the third phase. Attitude and position sensors were selected, tested, and integrated with the controller. Trajectory tracking, stability testing, and tethered testing were performed during this phase. A paper that reports the development of this phase is in preparation. In phase 4, we extended the previous work on the 3DOF controller design for the Quanser UFO to the 6DOF dynamic model based on the OU UFO structure. The 6DOF controller design was also based on the TLC scheme. The 3DOF controller that had been well tested on the 3DOF Quanser UFO was adapted to the OU UFO parameters and served as part of the 6DOF controller. The controller design and the simulation test results of the overall closed-loop system are presented in this paper. With the success of the previous phases, a HIL test of the 6DOF controller will be performed with a load cell during the fifth phase. Using the test data collected in phase 5, flight tests are planned for phase 6. The results of phases 5 and 6 will be presented in subsequent papers.

The paper is organized as follows. Following this Introductory section, Sec. II presents some technical preliminaries to facilitate the development of the main results. Section III describes the 6DOF model for the OU UFO. Section IV details the 6DOF TLC controller design. Section V presents the simulation verification of the 6DOF controller design. Section VI discusses the implementation of navigation system. Section VII concludes the paper with a summary of main results and discussion of needs for future work.

II. Technical Preliminaries

A. Trajectory Linearization Control

In this section, we briefly introduce the trajectory linearization control method, which will be used to design the 6DOF controller for the OU UFO. Consider the nonlinear dynamic system

$$\dot{\xi}(t) = f(\xi(t), \mu(t)), \qquad \eta(t) = h(\xi(t), \mu(t)) \tag{1}$$

where $\xi(t) \in \mathbb{R}^n$, $\mu(t) \in \mathbb{R}^l$, $\eta(t) \in \mathbb{R}^m$ are the state, input, and output, respectively, and the mappings $f(\cdot,\cdot)$:$\mathbb{R}^n \times \mathbb{R}^l \to \mathbb{R}^n$ and $h(\cdot,\cdot)$: $\mathbb{R}^n \times \mathbb{R}^l \to \mathbb{R}^m$ are bounded and locally Lipschitz. Let $\bar{\xi}(t)$, $\bar{\eta}(t)$, $\bar{\mu}(t)$ be the nominal state, nominal output trajectories, and nominal control satisfying

$$\dot{\bar{\xi}}(t) = f(\bar{\xi}(t), \bar{\mu}(t)) \qquad \bar{\eta}(t) = h(\bar{\xi}(t), \bar{\mu}(t)) \tag{2}$$

and define tracking errors by

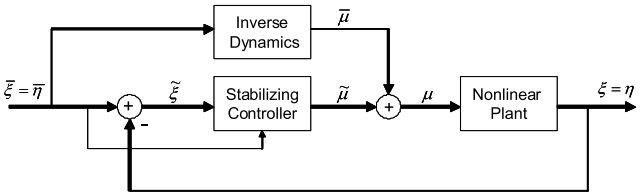

Fig. 3 State feedback TLC configuration.

$$\tilde{\xi}(t) = \xi(t) - \bar{\xi}(t), \qquad \tilde{\eta}(t) = \eta(t) - \bar{\eta}(t)$$
$$\tilde{\mu}(t) = \mu(t) - \bar{\mu}(t)$$

Then, the tracking error dynamics are governed by

$$\begin{aligned}\dot{\tilde{\xi}}(t) &= f(\bar{\xi}(t) + \tilde{\xi}(t), \bar{\mu}(t) + \tilde{\mu}(t)) - f(\bar{\xi}(t), \bar{\mu}(t)) \\ &= F(\tilde{\xi}(t), \tilde{\mu}(t), \bar{\xi}(t), \bar{\mu}(t)) \\ \tilde{\eta}(t) &= h(\bar{\xi}(t) + \tilde{\xi}(t), \bar{\mu}(t) + \tilde{\mu}(t)) - h(\bar{\xi}(t), \bar{\mu}(t)) \\ &= H(\tilde{\xi}(t), \tilde{\mu}(t), \bar{\xi}(t), \bar{\mu}(t)) \end{aligned} \tag{3}$$

As shown in Fig. 3, state trajectory linearization control consists of two parts: an open-loop dynamic inverse I/O mapping of the plant to compute the nominal control function $\bar{\mu}(t)$ for any given nominal output trajectory $\bar{\eta}(t)$, and a closed-loop tracking error stabilizing control law $\tilde{\mu}(\tilde{\xi}, \bar{\xi})$ to account for modeling simplifications and uncertainties, disturbances and excitation of internal dynamics.

The nominal control $\bar{\mu}$ can be designed using a nonlinear dynamic pseudoinversion technique [18]. The pseudoinverse is designed to be bounded-input–bounded-output stable to guarantee the boundedness of the nominal trajectories. With the assumption that the tracking errors are small by performance requirement, the tracking error dynamics can be linearized along the nominal trajectory as

$$\dot{x} = A_c(t)x + B_c(t)u \qquad y = C_c(t)x + D_c(t)u \tag{4}$$

where

$$A_c(t) = A(\bar{\xi}(t), \bar{\mu}(t)) = \frac{\partial}{\partial \xi} f(\xi, \mu)|_{\bar{\xi}, \bar{\mu}}$$
$$B_c(t) = B(\bar{\xi}(t), \bar{\mu}(t)) = \frac{\partial}{\partial \mu} f(\xi, \mu)|_{\bar{\xi}, \bar{\mu}}$$
$$C_c(t) = C(\bar{\xi}(t), \bar{\mu}(t)) = \frac{\partial}{\partial \xi} h(\xi, \mu)|_{\bar{\xi}, \bar{\mu}}$$
$$D_c(t) = D(\bar{\xi}(t), \bar{\mu}(t)) = \frac{\partial}{\partial \mu} h(\xi, \mu)|_{\bar{\xi}, \bar{\mu}}$$

which can be stabilized using a linear time-varying (LTV) stabilization control law, $u = K(t)x$, with the assumption that the system is strongly controllable. The LTV control gain $K(t)$ can be computed symbolically using the parallel differential eigenstructure (PD eigenstructure) assignment approach [18,19]. The overall controller is called a trajectory linearization controller [18].

The TLC combines nonlinear dynamic inversion and linear time-varying feedback stabilization in a novel way. Nonlinear tracking and decoupling control by trajectory linearization can be viewed as the ideal gain-scheduling controller designed at every point on the trajectory. Therefore, TLC provides robust stability without interpolation of controller gains. The theoretical research on TLC is presented in several publications [18,20,21], etc. In [18], a design of a tracking controller for a benchmark nonlinear plant using TLC is presented. Simulation case studies show that significant improvement in tracking performance, robustness, and disturbance rejection over the classical and modern gain scheduled controllers can be achieved using rational combinations of nonlinear and LTV control techniques. Regular perturbation analysis and singular perturbation analysis of the TLC approach are presented in [20,21]. TLC has been successfully applied to several applications, including the X33 Reusable Launch Vehicle Flight Controller [22–24], Quanser UFO Flight Control Test Bed [15–17], and Ohio University Robocup Robot Soccer Players [25]; thus, it is proven to be a promising new control method and worthy of further development and research.

B. Three-Degree-of-Freedom Controller for the Quanser UFO

As part of our development strategy, the design of a 3DOF attitude controller was first carried out for the Quanser UFO, which is constrained to rotational motions with only angular encoders as attitude measurement sensors. The Quanser platform allowed us to focus on the control algorithm design without concerning inertial attitude sensor issues. Once developed, the 3DOF attitude controller will become the inner loop for the 6DOF controller shown in Fig. 4. The 3DOF UFO attitude controller employed the TLC algorithm introduced in the preceding subsection. A detailed design was presented in [15–17] and will not be reviewed here for brevity. In our previous works, the gyroscopic effects of the propellers were not considered in the modeling, because the gyroscopic moments of the lightweight plastic propellers were 2 orders of magnitude less than the vehicle control moments, and, moreover, they were largely canceled due to the counter rotation of the propellers. Because the rotor gyroscopic effects created a (negligible) inertial coupling between the roll, pitch, and yaw channels, they were treated as a regular perturbation or parametric model uncertainty in the controller design.

III. Six-Degree-of-Freedom Modeling

Typical modern nonlinear flight control techniques employ the affine nonlinear state equation model

$$\dot{\boldsymbol{\xi}} = f(\boldsymbol{\xi}) + g(\boldsymbol{\xi})\boldsymbol{\mu} \qquad \boldsymbol{\eta} = c(\boldsymbol{\xi}) + d(\boldsymbol{\xi})\mu$$

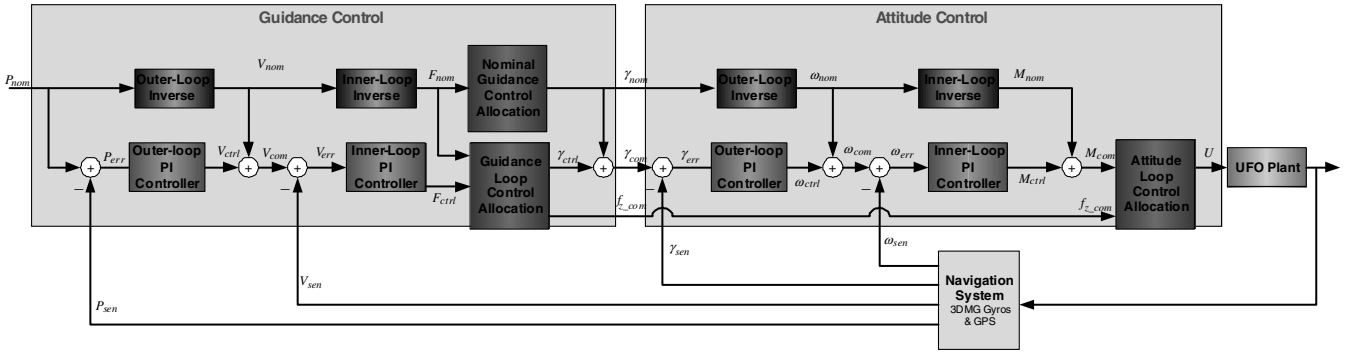

Fig. 4 Six-DOF trajectory linearization controller block diagram.

where $\boldsymbol{\xi}$ is the state vector, $\boldsymbol{\mu}$ is the control vector, and $\boldsymbol{\eta}$ is the output vector. The vector field f usually captures inertial and structural couplings, as well as aerodynamic and propulsion couplings of the state variables, whereas the vector field g represents effectiveness of the control effectors on the rate of change of the state variables. To maximize the crosscutting capability of our design for scaling or alteration of the airframe, or migration to different airframes, we choose to separate the inertial/structural dynamics from the aero/propulsive dynamics as

$$\dot{\boldsymbol{\xi}} = f_1(\boldsymbol{\xi}) + f_2(\boldsymbol{\xi}) + g(\boldsymbol{\xi})\mu$$

where $f_1(\boldsymbol{\xi})$ captures the inertial/structural dynamics due to vehicle mass properties and structural configuration that can be determined by mechanical analysis and testing, whereas $f_2(\boldsymbol{\xi})$ represents aerodynamic and propulsive forces and moments that are usually determined by computational fluid dynamics analysis, wind-tunnel testing, and flight data. The control design will first use $f_2(\boldsymbol{\xi})$ as virtual controls to achieve desired motion, then realize the virtual control commands as a (static) control allocation design.

The 6DOF UFO motion can be decomposed into translational motions and rotational motions; each of these motions is described by the dynamics and kinematics equations of motion (EOM) using the standard earth-fixed, body-carrying earth-fixed, and body-fixed reference frames, which can be found in, for example, [26], pp. 227–233. Because the TLC design is an analytical procedure, the EOMs are included here for convenience.

The kinematics equation for translational motion are given as

$$\dot{P} = \begin{bmatrix} C_\theta C_\psi & S_\phi S_\theta C_\psi - C_\phi S_\psi & C_\phi S_\theta C_\psi + S_\phi S_\psi \\ C_\theta S_\psi & S_\phi S_\theta S_\psi + C_\phi C_\psi & C_\phi S_\theta S_\psi - S_\phi C_\psi \\ -S_\theta & S_\phi C_\theta & C_\phi C_\theta \end{bmatrix} V = B_1(\gamma)V \tag{5}$$

where $C_* = \cos(*)$ and $S_* = \sin(*)$. The dynamics equations for translational motion are given as

$$\dot{V} = \begin{bmatrix} 0 & r & -q \\ -r & 0 & p \\ q & -p & 0 \end{bmatrix} V + \frac{1}{m}F = A_2(\omega)V + \frac{1}{m}F \tag{6}$$

The kinematics equations for rotational motion are given as

$$\dot{\gamma} = \begin{bmatrix} p + qS_\phi S_\theta / C_\theta + rC_\phi S_\theta / C_\theta \\ qC_\phi - rS_\phi \\ qS_\phi / C_\theta + rC_\phi / C_\theta \end{bmatrix} = B_3(\gamma)\omega \tag{7}$$

The dynamics equations for rotational motion are given as

$$\dot{\omega} = \begin{bmatrix} I^p_{pq} pq + I^p_{qr} qr \\ I^q_{pp} p^2 + I^q_{rr} r^2 + I^q_{pr} pr \\ I^r_{pq} pq + I^r_{qr} qr \end{bmatrix} + \begin{bmatrix} g^p_l & 0 & g^p_n \\ 0 & g^q_m & 0 \\ g^r_l & 0 & g^r_n \end{bmatrix} M \tag{8}$$

where the coefficients I^*_{**} and g^*_* are defined by the mass moments of inertia of the airframe $I_{xx}, I_{yy}, I_{zz}, I_{xz}$, and are given in the Appendix. In these equations, the force F and moment M are used as virtue controls.

IV. Six-Degree-of-Freedom Controller Design

The controller for the 6DOF UFO takes position trajectory commands and calculates the corresponding voltage values for the UFO motors and deflection angle of the yaw flaps such that the UFO tracks the designated guidance trajectory. The controller consists of two parts, guidance control and attitude control, which control the translational motion and rotational motion of the UFO, respectively. The two subsystems are connected by the control allocation of the guidance control system, which takes the desired force from the output of the guidance controller as its input and provides the command for the attitude control system. The block diagram of the closed-loop system is illustrated in Fig. 4.

The overall closed-loop system consists of four loops, each of which has the complete TLC structure shown in Fig. 3. The two loops that are together, closer to the plant, are called attitude control; the other two loops that are together are called guidance control, as illustrated in Fig. 4. From the innermost loop in Fig. 4, the block labeled Inner-Loop Inverse and the block labeled Inner-Loop PI Controller (where PI stands for proportional-integral) of the attitude control part correspond to the Inverse Dynamics and Stabilizing Controller blocks in Fig. 3, respectively; the Attitude Loop Control Allocation block together with the UFO Plant block correspond to the Nonlinear Plant block in Fig. 3. Accordingly, for the other three loops, each loop has its own inverse and feedback controller blocks, and the inner loop of each loop constitutes its nonlinear plant.

The design of the attitude controller is presented in [15–17]. The guidance control system design adopts the same control scheme as used for the attitude control, thus, in this section, the design procedure will be introduced briefly. The focus will be on presenting the final design results, integration of the two subsystems, and design of the control allocations. Because the OU UFO is still under construction, the 6DOF controller design and simulation testing are based on some estimated model parameters. Because the TLC design is a model-based, analytical approach, the controller should be readily applied to the OU UFO when actual model parameters become available.

A. Guidance Controller

The guidance controller consists of two loops, an outer loop and an inner loop, which control the position and body velocity of the UFO, respectively. The guidance controller takes in position command and calculates attitude command for attitude control loop as well as the total thrust force.

1. *Outer-Loop Control*

The outer loop of the guidance control takes in position command and position measurement to calculate velocity command for the inner loop. It has a dynamic inversion and a stabilizing controller as shown in the leftmost two blocks of Fig. 4.

We start our design from the dynamic inversion. The nominal body velocity is obtained from the kinematics Eqs. (5) for translational motion as $V_{\text{nom}} = B_1^{-1}(\gamma_{\text{nom}})\dot{P}_{\text{nom}}$, where $B_1(\gamma_{\text{nom}})$ is the matrix in Eq. (5) with ϕ, θ, ψ replaced with their respective nominal values $\phi_{\text{nom}}, \theta_{\text{nom}}, \psi_{\text{nom}}$, which are computed by the guidance control allocation to be designed in the sequel, and $\dot{P}_{\text{nom}}$ is obtained from the position command P_{com} using a pseudodifferentiator with a transfer function

$$G_{\text{diff}}(s) = \frac{\omega^2_{n,\text{diff}} s}{s^2 + 2\zeta_{\text{diff}}\omega_{n,\text{diff}} s + \omega^2_{n,\text{diff}}} \tag{9}$$

We then proceed to define the error dynamics and design the stabilizing controller. Define the position tracking error** as $P_{\text{err}} = P_{\text{sen}} - P_{\text{com}}$. The error dynamics are given by $\dot{P}_{\text{err}} = B_1(\gamma_{\text{nom}})V_{\text{ctrl}}$. The proportional-integral feedback control law for the position loop is given by

$$V_{\text{ctrl}} = -K_{P_1}(t)P_{\text{err}} - K_{I_1}(t)\int P_{\text{err}}$$

where the PI gain matrices are designed using the PD-eigenvalue assignment procedure as

**Note that the tracking errors defined here and in the sequel are the negative of those shown in Fig. 4.

$$K_{I_1}(t) = -B_1^{-1}(\gamma_{\text{nom}})A_{1\cdot 1} = \begin{bmatrix} \alpha_{111}C_{\theta_n}C_{\psi_n} & \alpha_{121}C_{\theta_n}S_{\psi_n} & -\alpha_{131}S_{\theta_n} \\ \alpha_{111}(S_{\phi_n}S_{\theta_n}C_{\psi_n} - C_{\phi_n}S_{\psi_n}) & \alpha_{121}(S_{\phi_n}S_{\theta_n}S_{\psi_n} + C_{\phi_n}C_{\psi_n}) & \alpha_{131}S_{\phi_n}C_{\theta_n} \\ \alpha_{111}(C_{\phi_n}S_{\theta_n}C_{\psi_n} + S_{\phi_n}S_{\psi_n}) & \alpha_{121}(C_{\phi_n}S_{\theta_n}S_{\psi_n} - S_{\phi_n}C_{\psi_n}) & \alpha_{131}C_{\phi_n}C_{\theta_n} \end{bmatrix}$$

$$K_{P_1}(t) = -B_1^{-1}(\gamma_{\text{nom}})A_{1\cdot 2} = \begin{bmatrix} \alpha_{112}C_{\theta_n}C_{\psi_n} & \alpha_{122}C_{\theta_n}S_{\psi_n} & -\alpha_{132}S_{\theta_n} \\ \alpha_{112}(S_{\phi_n}S_{\theta_n}C_{\psi_n} - C_{\phi_n}S_{\psi_n}) & \alpha_{122}(S_{\phi_n}S_{\theta_n}S_{\psi_n} + C_{\phi_n}C_{\psi_n}) & \alpha_{132}S_{\phi_n}C_{\theta_n} \\ \alpha_{112}(C_{\phi_n}S_{\theta_n}C_{\psi_n} + S_{\phi_n}S_{\psi_n}) & \alpha_{122}(C_{\phi_n}S_{\theta_n}S_{\psi_n} - S_{\phi_n}C_{\psi_n}) & \alpha_{132}C_{\phi_n}C_{\theta_n} \end{bmatrix}$$

where

$$A_{1\cdot k} = \text{diag}[-\alpha_{11k}(t), \quad -\alpha_{12k}(t), \quad -\alpha_{13k}(t)] \qquad k = 1, 2$$

are time-varying controller parameter matrices representing the desired closed-loop dynamics, and α_{ijk} with $i = 1$ are chosen as

$$\alpha_{ij1}(t) = \omega_{n,j}^2(t), \qquad \alpha_{i,j,2}(t) = 2\zeta_j\omega_{n,j}(t) - \frac{\dot{\omega}_{n,j}(t)}{\omega_{n,j}(t)} \tag{10}$$

where $\omega_{n,j}(t)$ are time-varying natural frequencies, and ζ_j are the constant damping ratios of the desired dynamics of each channel $j = 1, 2, 3$, representing roll, pitch, and yaw channels, respectively. Here and in the sequel, we will use $i = 1, 2, 3, 4$ as in K_{P_i}, K_{I_i}, $A_{i\cdot k}$, and α_{ijk} to index the four TLC control loops as shown in Fig. 4, counting from the outermost loop (the position loop). The output of the outer-loop controller is the velocity command given by

$$V_{\text{com}} = V_{\text{nom}} + V_{\text{ctrl}}$$

2. Inner-Loop Control

The inner loop of the guidance control takes in velocity command and velocity measurement to calculate force command for the guidance loop control allocation. It has a dynamic inversion and a stabilizing controller, as shown in the second loop from the left in Fig. 4.

We start our design from the dynamic inversion. The nominal force is calculated from the dynamics Eqs. (6) of translational motion as

$$\begin{bmatrix} F_{x_{\text{nom}}} \\ F_{y_{\text{nom}}} \\ F_{z_{\text{nom}}} \end{bmatrix} = m\begin{bmatrix} \dot{u}_{\text{nom}} + q_{\text{nom}}w_{\text{nom}} - r_{\text{nom}}v_{\text{nom}} \\ \dot{v}_{\text{nom}} + r_{\text{nom}}u_{\text{nom}} - p_{\text{nom}}w_{\text{nom}} \\ \dot{w}_{\text{nom}} + p_{\text{nom}}v_{\text{nom}} - q_{\text{nom}}u_{\text{nom}} \end{bmatrix}$$

where

$$\dot{V}_{\text{nom}} = [\dot{u}_{\text{nom}}, \quad \dot{v}_{\text{nom}}, \quad \dot{w}_{\text{nom}}]^T$$

are obtained from V_{nom} using the pseudodifferentiator (9).

Next, we define the error dynamics and design the stabilizing controller. The error dynamics of the body velocity are given by

$$\dot{V}_{\text{err}} = A_2(\omega_{\text{nom}})V_{\text{err}} + \frac{1}{m}F_{\text{ctrl}}$$

where

$$V_{\text{err}} = [u_{\text{err}} \quad v_{\text{err}} \quad w_{\text{err}}]^T = V_{\text{sen}} - V_{\text{nom}}$$

$$F_{\text{ctrl}} = [F_{x_{\text{ctrl}}} \quad F_{y_{\text{ctrl}}} \quad F_{z_{\text{ctrl}}}]$$

and $A_2(\omega_{\text{nom}})$ is the matrix in Eq. (6) with p, q, r replaced by p_{nom}, q_{nom}, r_{nom}, respectively. The inner-loop feedback control is given by

$$F_{\text{ctrl}} = -K_{P2}(t)V_{\text{err}} - K_{I2}(t)\int V_{\text{err}}$$

The body velocity loop PI feedback gain matrices are given by

$$K_{P_2}(t) = m[A_2(\omega_{\text{nom}}) - A_{2\cdot 2}] = m\begin{bmatrix} \alpha_{212} & r_{\text{nom}} & -q_{\text{nom}} \\ -r_{\text{nom}} & \alpha_{222} & p_{\text{nom}} \\ q_{\text{nom}} & -p_{\text{nom}} & \alpha_{232} \end{bmatrix}$$

$$K_{I_2}(t) = -mA_{2\cdot 1} = m\begin{bmatrix} \alpha_{211} & 0 & 0 \\ 0 & \alpha_{221} & 0 \\ 0 & 0 & \alpha_{231} \end{bmatrix}$$

and the inner-loop controller output are F_{nom} and F_{ctrl}, respectively.

3. Guidance Control Allocation

It is noted that, with the total body force as virtual control input, the TLC controllers for the position and velocity loops are generic for any 3DOF rigid-body translational motions. It is how the body force is generated that distinguishes this vehicle configuration from others. The UFO generates the total body force that is required to fly the trajectory by vectoring its body-fixed thrust vector using attitude maneuvers. The guidance control allocation unit takes as its input the thrust force vector and calculates the Euler attitude angles and the total thrust along the body z axis as its output.

Because the propellers are in a body-fixed configuration, only vertical propulsive force f_z can be generated. Therefore, the propulsive forces f_x and f_y are zero.[††] Thus, body forces are given by

$$F_x = -mgS_\theta - C_{D_V}u^2 \qquad F_y = mgC_\theta S_\phi - C_{D_V}v^2$$
$$F_z = f_z + mgC_\theta C_\phi - C_{D_V}w^2 \tag{11}$$

where C_{D_V} is a coefficient of drag force due to velocity in units of $\text{N}\cdot\text{s}^2/\text{m}^2$. The conventional drag coefficient C_{D_α} for a winged aircraft is the derivative of the drag force with respect to angle of attack, because the drag force is mainly due to the resultant aerodynamic force in generating lift. The current OU UFO design is a very slow flyer, and it does not have much lifting surface, therefore it is assumed that the drag force is mainly due to parasite drag, which is independent of angle of attack. For simplicity, we further assume that the drag force is proportional to velocity squared and, considering the cruising pitch angle is very small, less than 1 deg, the drag force is expressed in the body-fixed frame. It is noted that the drag model as presented is a gross simplification of the actual vehicle in flight, but it should suffice for the purpose of a proof-of-concept controller design. Any subsequent improvements to the drag model can be readily incorporated into the controller, owing to the analytical nature of the TLC design.

To avoid unintended feedback loops, the guidance control allocation must calculate separately the nominal attitude command γ_{nom} and corrective attitude command γ_{ctrl} due to feedback control. First, we solve the nominal Euler attitude γ_{nom} by inverting the force model (11) as follows:

[††]The flaps on the OU UFO can generate side force f_y when actuated collectively. This capability is not used in the present design, but will be implemented in future development of the controller.

$$\phi_{\text{nom}} = \text{asin}\left(\frac{F_{y_{\text{nom}}} + C_{D_V} v_{\text{nom}}^2}{\sqrt{m^2 g^2 - (F_{x_{\text{nom}}} + C_{D_V} u_{\text{nom}}^2)^2}}\right)$$

$$\theta_{\text{nom}} = \text{asin}\left(-\frac{F_{x_{\text{nom}}} + C_{D_V} u_{\text{nom}}^2}{mg}\right)$$

$$\psi_{\text{nom}} = \begin{cases} \tan^{-1}\left(\frac{\dot{y}_{\text{nom}}}{\dot{x}_{\text{nom}}}\right) & |\dot{x}_{\text{nom}}| \geq 0.001 \quad \text{and} \quad |\dot{y}_{\text{nom}}| \geq 0.001 \\ \text{hold}\psi_{\text{nom}} & \text{otherwise} \end{cases}$$

Note from Eq. (11) that the total force vector in the body-fixed frame does not depend on yaw angle. Thus, ψ_{nom} can be assigned to any value. However, from practical concern, yaw angle is assigned to the heading angle so that the x axis of the UFO will always be aligned with the heading direction. The dead-zone function applied to the ψ_{nom} equation is to prevent ψ_{nom} from jumping from one quadrant to another when $|\dot{x}_{\text{nom}}|$ and $|\dot{y}_{\text{nom}}|$ jitters near zero.

The corrective attitude command is computed by inverting the Jacobian of the first two equations in Eq. (11) at the nominal state, which is given by

$$\begin{bmatrix} \phi_{\text{ctrl}} \\ \theta_{\text{ctrl}} \end{bmatrix} = \frac{1}{mg} \begin{bmatrix} -\sec(\theta_{\text{nom}})\tan(\theta_{\text{nom}})\tan(\phi_{\text{nom}}) & \sec(\theta_{\text{nom}})\sec(\phi_{\text{nom}}) \\ -\sec(\theta_{\text{nom}}) & 0 \end{bmatrix} \times \begin{bmatrix} F_{x_{\text{ctrl}}} \\ F_{y_{\text{ctrl}}} \end{bmatrix}$$

It is noted that ψ_{nom} does not need feedback correction at this stage. The total attitude command that goes into the attitude controller is then given by

$$\gamma_{\text{com}} = [\,\phi_{\text{nom}} + \phi_{\text{ctrl}} \quad \theta_{\text{nom}} + \theta_{\text{ctrl}} \quad \psi_{\text{nom}}\,]^T$$

The total thrust force command $f_{z_{\text{com}}}$ need not be separated into the nominal and corrective either, as it goes directly to the actuator. The command $f_{z_{\text{com}}}$ is computed by inverting the third equation in Eq. (11) as

$$f_{z_{\text{com}}} = F_{z_{\text{com}}} + C_{D_V} w^2 - \sqrt{m^2 g^2 - (F_{x_{\text{com}}} + C_{D_V} u^2)^2 - (F_{y_{\text{com}}} + C_{D_V} v^2)^2}$$

B. Attitude Controller

The attitude controller consists of two loops, an outer loop and an inner loop, which control the attitude and body rate of the UFO, respectively. The attitude controller takes in attitude command from the guidance loop and calculates voltage command for the UFO. The detailed attitude controller design can be found in [15–17], and the design procedure is very similar to the guidance loop. Here, we only summarize the design results.

1. *Outer-Loop Control*

The outer loop of the attitude control takes in attitude command and attitude measurement to calculate the body rate command for the inner loop. It has a dynamic inversion and a stabilizing controller as shown in the third loop from the left in Fig. 4.

We start our design from the dynamic inversion. The nominal body rates are obtained from inverting the rotational kinematics Eq. (7) as

$$p_{\text{nom}} = \dot{\phi}_{\text{nom}} - \dot{\psi}_{\text{nom}} \sin(\theta_{\text{nom}})$$
$$q_{\text{nom}} = \dot{\theta}_{\text{nom}} \cos(\phi_{\text{nom}}) + \dot{\psi}_{\text{nom}} \sin(\phi_{\text{nom}}) \cos(\theta_{\text{nom}})$$
$$r_{\text{nom}} = -\dot{\theta}_{\text{nom}} \sin(\phi_{\text{nom}}) + \dot{\psi}_{\text{nom}} \cos(\phi_{\text{nom}}) \cos(\theta_{\text{nom}})$$

where $\dot{\phi}_{\text{nom}}$, $\dot{\theta}_{\text{nom}}$, $\dot{\psi}_{\text{nom}}$ are obtained from ϕ_{nom}, θ_{nom}, ψ_{nom} using the pseudodifferentiator (9).

The tracking control law for outer-loop proportional-integral feedback is

$$\omega_{\text{ctrl}} = -K_{P3}(t)\gamma_{\text{err}} - K_{I3}(t)\int \gamma_{\text{err}}$$

where the attitude tracking error $\gamma_{\text{err}} = \gamma_{\text{sen}} - \gamma_{\text{com}}$, and the outer-loop PI feedback control gain matrices are

$$K_{P3}(t) = \begin{bmatrix} \alpha_{312} & q_{\text{nom}} S_{\phi_n} + r_{\text{nom}} C_{\phi_n} & -\alpha_{332} S_{\theta_n} \\ -r_{\text{nom}} & \alpha_{322} C_{\phi_n} + \frac{S_{\theta_n}[q_{\text{nom}} S_{\phi_n} + r_{\text{nom}} C_{\phi_n}] S_{\phi_n}}{C_{\theta_n}} & \alpha_{332} S_{\phi_n} C_{\theta_n} \\ q_{\text{nom}} & -\alpha_{322} S_{\phi_n} + \frac{S_{\theta_n}[q_{\text{nom}} S_{\phi_n} + r_{\text{nom}} C_{\phi_n}] C_{\phi_n}}{C_{\theta_n}} & \alpha_{332} C_{\phi_n} C_{\theta_n} \end{bmatrix}$$

$$K_{I3}(t) = \begin{bmatrix} \alpha_{311} & 0 & -\alpha_{331} S_{\theta_n} \\ 0 & \alpha_{321} C_{\phi_n} & \alpha_{331} S_{\phi_n} C_{\theta_n} \\ 0 & -\alpha_{321} S_{\phi_n} & \alpha_{331} C_{\phi_n} C_{\theta_n} \end{bmatrix}$$

The output of the attitude outer-loop controller is given by

$$\omega_{\text{com}} = \omega_{\text{nom}} + \omega_{\text{ctrl}}$$

2. *Inner-Loop Control*

The inner loop of the attitude control takes in body rate command and body rate measurement to calculate torque command for the attitude loop control allocation. It has a dynamic inversion and a stabilizing controller as shown in the fourth loop from the left in Fig. 4.

We start our design from the dynamic inversion. The nominal body torque are calculated by inverting the rotational dynamics Eq. (8),

$$M_{x_{\text{nom}}} = I_{xx}\dot{p}_{\text{nom}} + (I_{zz} - I_{yy}) q_{\text{nom}} r_{\text{nom}} - I_{xz}(\dot{r}_{\text{nom}} + q_{\text{nom}} p_{\text{nom}})$$
$$M_{y_{\text{nom}}} = I_{yy}\dot{q}_{\text{nom}} + (I_{xx} - I_{zz}) p_{\text{nom}} r_{\text{nom}} + I_{xz}(p_{\text{nom}}^2 - r_{\text{nom}}^2)$$
$$M_{z_{\text{nom}}} = I_{zz}\dot{r}_{\text{nom}} + (I_{yy} - I_{xx}) q_{\text{nom}} p_{\text{nom}} + I_{xz}(q_{\text{nom}} r_{\text{nom}} - \dot{p}_{\text{nom}})$$

where $\dot{p}_{\text{nom}}$, $\dot{q}_{\text{nom}}$, $\dot{r}_{\text{nom}}$ are obtained from p_{nom}, q_{nom}, r_{nom} using the pseudodifferentiator (9).

The PI control law for the inner loop is given by

$$M_{\text{ctrl}} = -K_{P4}(t)\omega_{\text{err}} - K_{I4}(t)\int \omega_{\text{err}}$$

where the attitude tracking error $\omega_{\text{err}} = \omega_{\text{sen}} - \omega_{\text{com}}$, and the inner-loop PI feedback control gain matrices are

$$K_{P4}(t) = \begin{bmatrix} I_{xx}(I_{pq}^p q_{\text{nom}} + \alpha_{412}) - I_{xz} I_{pq}^r q_{\text{nom}} & I_{xx}(I_{pq}^p p_{\text{nom}} + I_{qr}^p r_{\text{nom}}) - I_{xz}(I_{pq}^r p_{\text{nom}} + I_{qr}^r r_{\text{nom}}) & I_{xx} I_{qr}^p q_{\text{nom}} - I_{xz}(I_{qr}^r q_{\text{nom}} + \alpha_{432}) \\ I_{yy}(2I_{pp}^q p_{\text{nom}} + I_{pr}^q r_{\text{nom}}) & I_{yy}\alpha_{422} & I_{yy}(2I_{rr}^q r_{\text{nom}} + I_{pr}^q p_{\text{nom}}) \\ -I_{xz}(I_{pq}^p q_{\text{nom}} + \alpha_{412}) + I_{zz} I_{pq}^r q_{\text{nom}} & -I_{xz}(I_{pq}^p p_{\text{nom}} + I_{qr}^p r_{\text{nom}}) + I_{zz}(I_{pq}^r p_{\text{nom}} + I_{qr}^r r_{\text{nom}}) & -I_{xz} I_{qr}^p q_{\text{nom}} + I_{zz}(I_{qr}^r q_{\text{nom}} + \alpha_{432}) \end{bmatrix}$$

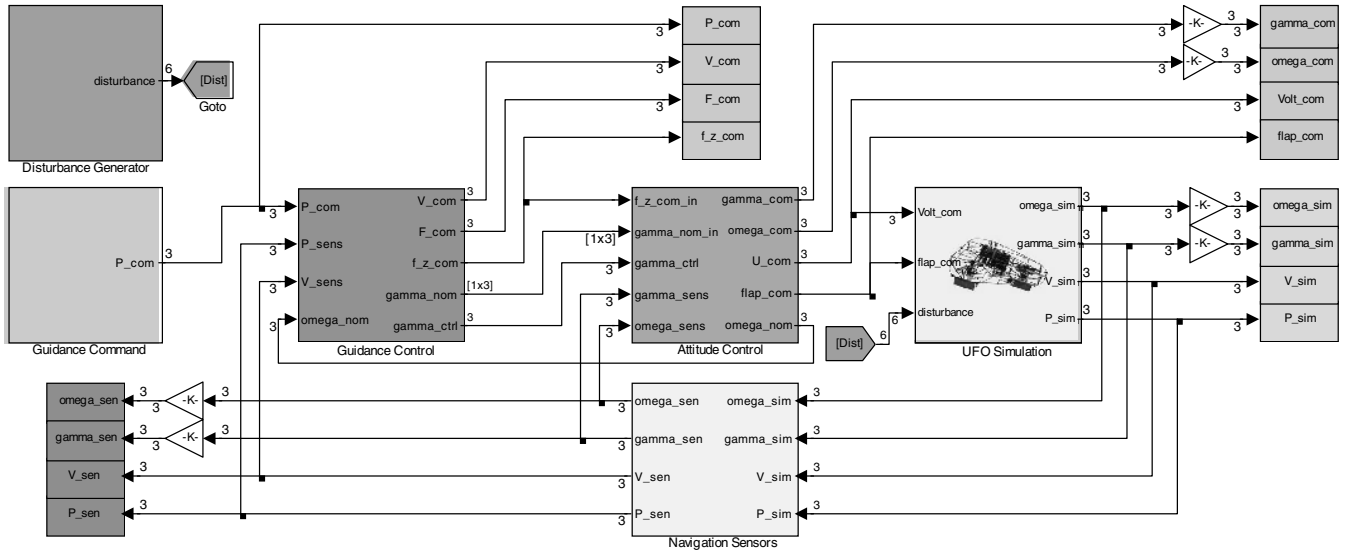

Fig. 5 SIMULINK setup of 6DOF simulation for command profile tracking.

$$K_{I4}(t) = \begin{bmatrix} I_{xx}\alpha_{411} & 0 & -I_{xz}\alpha_{431} \\ 0 & I_{yy}\alpha_{421} & 0 \\ -I_{xz}\alpha_{411} & 0 & I_{zz}\alpha_{431} \end{bmatrix}$$

The output of the inner-loop controller is given by

$$M_{\text{com}} = M_{\text{nom}} + M_{\text{ctrl}}$$

3. Attitude Control Allocation

The actuator command

$$U_{\text{com}} = [\, U_{1_{\text{com}}} \quad U_{2_{\text{com}}} \quad U_{3_{\text{com}}} \quad U_{4_{\text{com}}} \,]^T$$

which consists of voltages applied to the three dc motors U_1, U_2, U_3 and the yaw trim flap deflection angle U_4 is determined from the moment command

$$M_{\text{com}} = [\, M_{x_{\text{com}}} \quad M_{y_{\text{com}}} \quad M_{z_{\text{com}}} \,]^T$$

calculated from attitude loop, and $f_{z_{\text{com}}}$ calculated from guidance loop control allocation. More specifically, the voltages of the three motors are determined by the roll and pitch moment and the thrust force; the yaw trim control U_4 is calculated based on the difference between the yaw moment $M_{z_{\text{com}}}$ needed to maintain the commanded yaw angle and the yaw moment produced by the propellers driven by the dc motors. It is noted that the front propeller is a reversed-pitch propeller that spins in the opposite direction of the rear propellers to generate thrust in the same direction, while canceling most of the reactive moments generated by the rear propellers, and the center of gravity is at the midpoint of the distance between the front and rear motors.

The moments and total thrust generated by the voltages applied to the three motors and the yaw trim flap deflection angle, respectively, are determined experimentally as

$$[\, M_x \quad M_y \quad M_z \quad f_z \,]^T = L[\, U_1 \quad U_2 \quad U_3 \quad U_4 \,]^T$$

where

$$L = \begin{bmatrix} \frac{\partial M_x}{\partial U_1} & \frac{\partial M_x}{\partial U_2} & \frac{\partial M_x}{\partial U_3} & \frac{\partial M_x}{\partial U_4} \\ \frac{\partial M_y}{\partial U_1} & \frac{\partial M_y}{\partial U_2} & \frac{\partial M_y}{\partial U_3} & \frac{\partial M_y}{\partial U_4} \\ \frac{\partial M_z}{\partial U_1} & \frac{\partial M_z}{\partial U_2} & \frac{\partial M_z}{\partial U_3} & \frac{\partial M_z}{\partial U_4} \\ \frac{\partial f_z}{\partial U_1} & \frac{\partial f_z}{\partial U_2} & \frac{\partial f_z}{\partial U_3} & \frac{\partial f_z}{\partial U_4} \end{bmatrix} = \begin{bmatrix} 0 & -0.991 & 0.991 & 0 \\ 0.569 & 0.582 & 0.582 & 0 \\ -0.106 & -0.106 & -0.106 & 0.1 \\ 1.120 & -1.120 & -1.120 & 0 \end{bmatrix}$$

Hence, the actuator commands are given by

$$\begin{bmatrix} U_{1_{\text{com}}} \\ U_{2_{\text{com}}} \\ U_{3_{\text{com}}} \\ U_{4_{\text{com}}} \end{bmatrix} = L^{-1} \begin{bmatrix} M_{x_{\text{com}}} \\ M_{y_{\text{com}}} \\ M_{z_{\text{com}}} \\ f_{z_{\text{com}}} \end{bmatrix}$$

V. Simulation and Results

The 6DOF controller and the UFO model are implemented in MATLAB/SIMULINK as shown in Fig. 5. The UFO model is implemented based on Eqs. (5–8) and (11) with actuator dynamics for each motor-propeller modeled as a second-order lowpass filter with a damping coefficient $\zeta = 0.707$ and $\omega_n = 30$. The system parameters are based on the OU UFO shown in Fig. 1a with $m = 6$ kg, $I_{xx} = 0.04012\ \text{kg} \cdot \text{m}^2$, $I_{yy} = 0.05288\ \text{kg} \cdot \text{m}^2$, $I_{zz} = 0.09014\ \text{kg} \cdot \text{m}^2$, $I_{xz} = 0.0002\ \text{kg} \cdot \text{m}^2$, and $C_{D_y} = 0.02$. The controller is implemented according to the design in Sec. IV. There are four (three-channel) pseudodifferentiators in the nominal controllers, and four LTV tracking error regulators in the overall closed-loop systems, as shown in Fig. 4.

For the present work, constant controller parameters α_{ijk} are used for $i = 1, 2, 3, 4$, $j = 1, 2, 3$, and $k = 1, 2$, as defined in Eq. (10), which define linear time invariant closed-loop dynamics for each of the four TLC loops described by the characteristic equation $\lambda^2 + 2\zeta\omega_n\lambda + \omega_n^2 = 0$. The parameters ζ and ω_n are shown in Table 2, where the damping coefficients ζ were set to 1.414 for all

Table 2 Controller coefficients

	Guidance outer loop, $i = 1$	Guidance inner loop, $i = 2$	Attitude outer loop, $i = 3$	Attitude inner loop, $i = 4$
ω_n	[0.094 0.07 0.088]	[0.375 0.281 0.35]	[1.5 1.125 1.4]	[6 4.5 5.6]
ζ	[$\sqrt{2}$ $\sqrt{2}$ $2\sqrt{2}$]	[$\sqrt{2}$ $\sqrt{2}$ $2\sqrt{2}$]	[$\sqrt{2}$ $\sqrt{2}$ $\sqrt{2}$]	[$\sqrt{2}$ $\sqrt{2}$ $\sqrt{2}$]

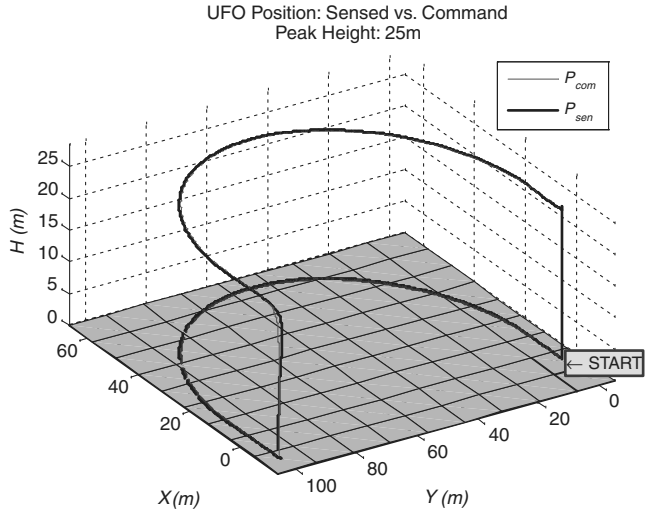

Fig. 6 Command profile tracking performance.

loops and all channels except for the z channel of the position and velocity loops. Overdamping was preferred because overshoot in position and velocity would cause the vehicle to oscillate in roll and pitch, and heavier damping was applied to the z channel to further minimize overshoot that might affect safe landing. The natural frequency ω_n for the body rate loop ($i = 4$) was chosen based on experience with the Quanser UFO [15,17], which should be sufficiently smaller than the actuator bandwidth and the plant bandwidth. As a starting point, the natural frequency ω_n for the Euler angle loop and guidance control loops were simply scaled down 4 times lower than its inner one. Note that the closed-loop bandwidth, which is proportional to ω_n, can be chosen as a function of time $\omega_n(t)$ to facilitate adaptive control for real-time tradeoff of performance vs robustness and energy consumption, which will be explored in future work. The natural frequency ω_n and damping ratio ζ of the pseudodifferentiators in the nominal controllers were chosen to be 5 rad/s and 1.414, respectively, for each channel in each loop except for the angular rate loop, where the natural frequency was chosen to be 10 rad/s. The current implementation does not use these pseudo-differentiators for command shaping filtering, and so the ω_n is selected only for desired noise filtering effects.

The tracking command of the simulation was generated for the following scenario: the UFO took off vertically and rose to a height of 24 m. It flew a semicircular arc with a turning radius of 50 m at this altitude, then landed vertically. The total flight time was 100 s. The peak commanded VTOL climb rate was about 3.5 m/s, and the commanded cruise speed was 3 m/s. Three simulation test cases were performed and presented here: 1) nominal design, 2) nominal design with force and torque disturbance, and 3) nominal design with loop delays.

Case 1: The nominal simulation results are presented in Figs. 6–12. Figure 6 shows the 3D view of the trajectory command and vehicle position along with the ground track. Figure 7 shows the position tracking performance for each state variable, exhibiting smooth transient and small tracking errors. The velocity trajectory tracking performance is shown in Fig. 8. The velocity command is generated by the nominal velocity command and position feedback controller. The longitudinal and lateral velocity $u(t)$ and $v(t)$ exhibit 15 and 50% overshoot, respectively, which do not have adverse effects on the position tracking. It is noted that the vehicle as simulated does not have side force control effector. The controller rolls the vehicle to create the desired lateral velocity using lift thrust and gravity automatically. In future work, the yaw flaps will be actuated collectively to generate side force, which should help to improve lateral velocity tracking, particularly for station keeping. The normal velocity $w(t)$ tracks exceptionally well. The guidance controller commands the attitude angles to vector the thrust. The attitude and angular rate tracking performances are shown in Figs. 9 and 10, respectively, which are very good. The actuator commands are shown in Fig. 11, which are smooth and within expected ranges.

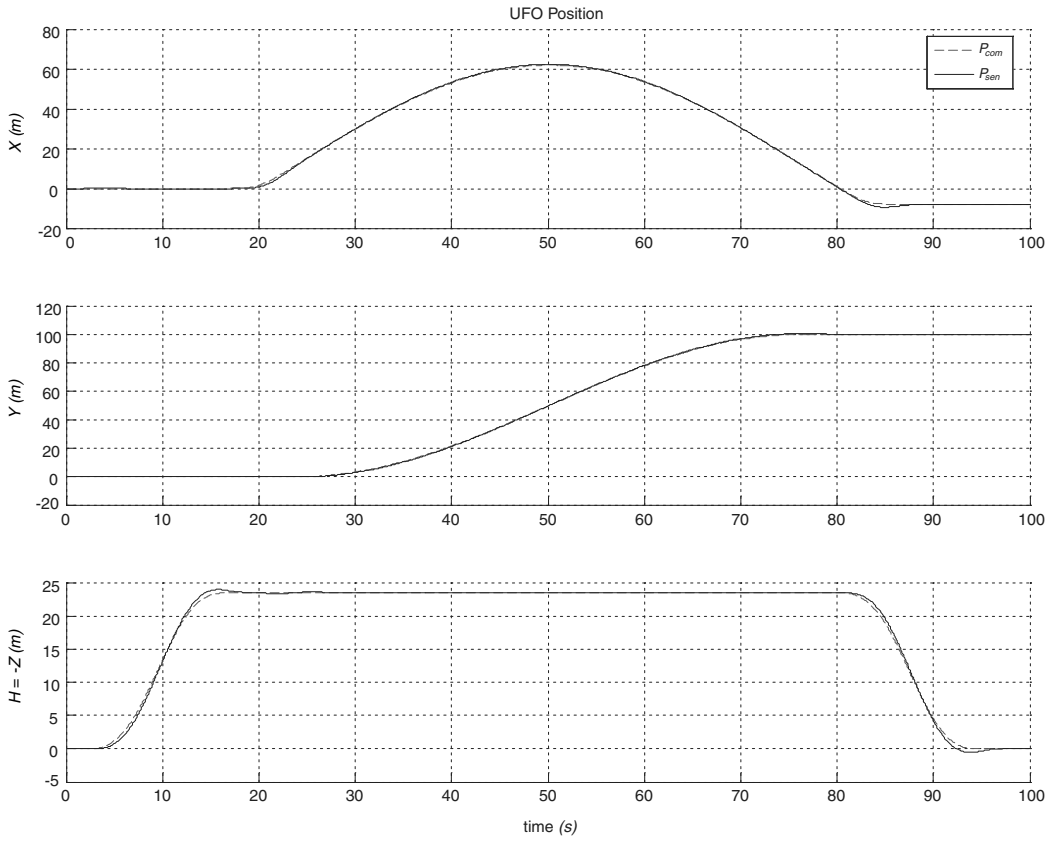

Fig. 7 Position response of command profile tracking.

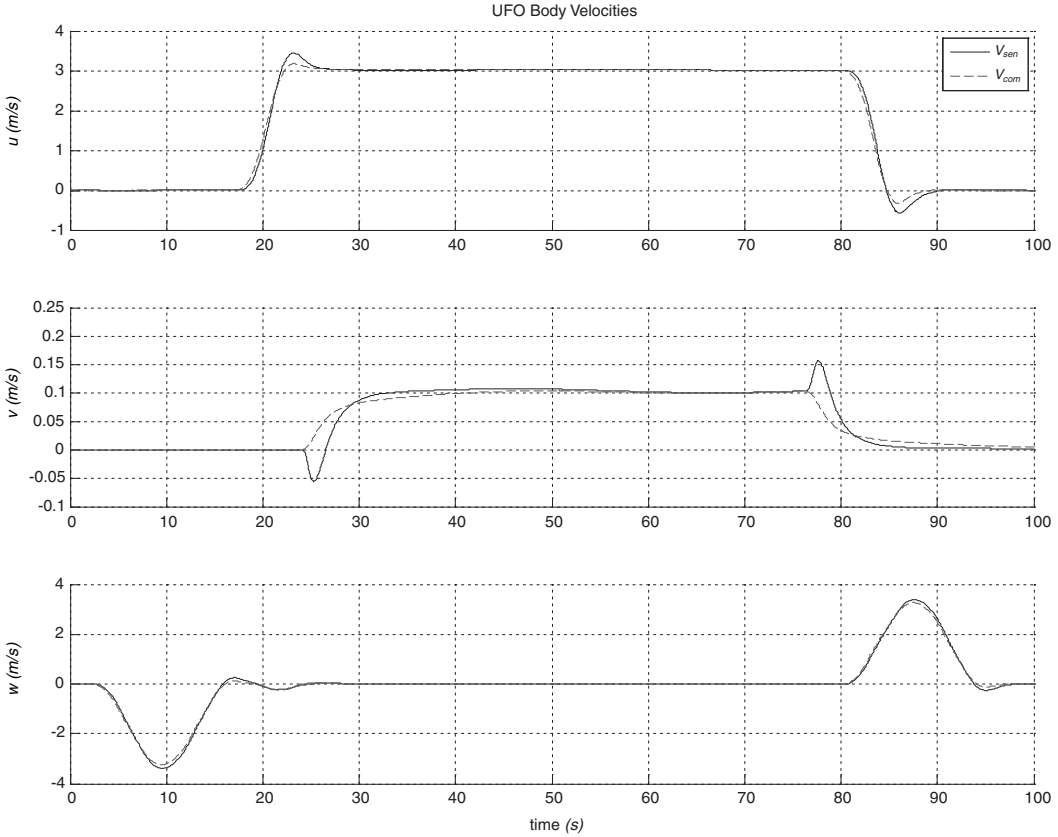

Fig. 8 Velocity response of command profile tracking.

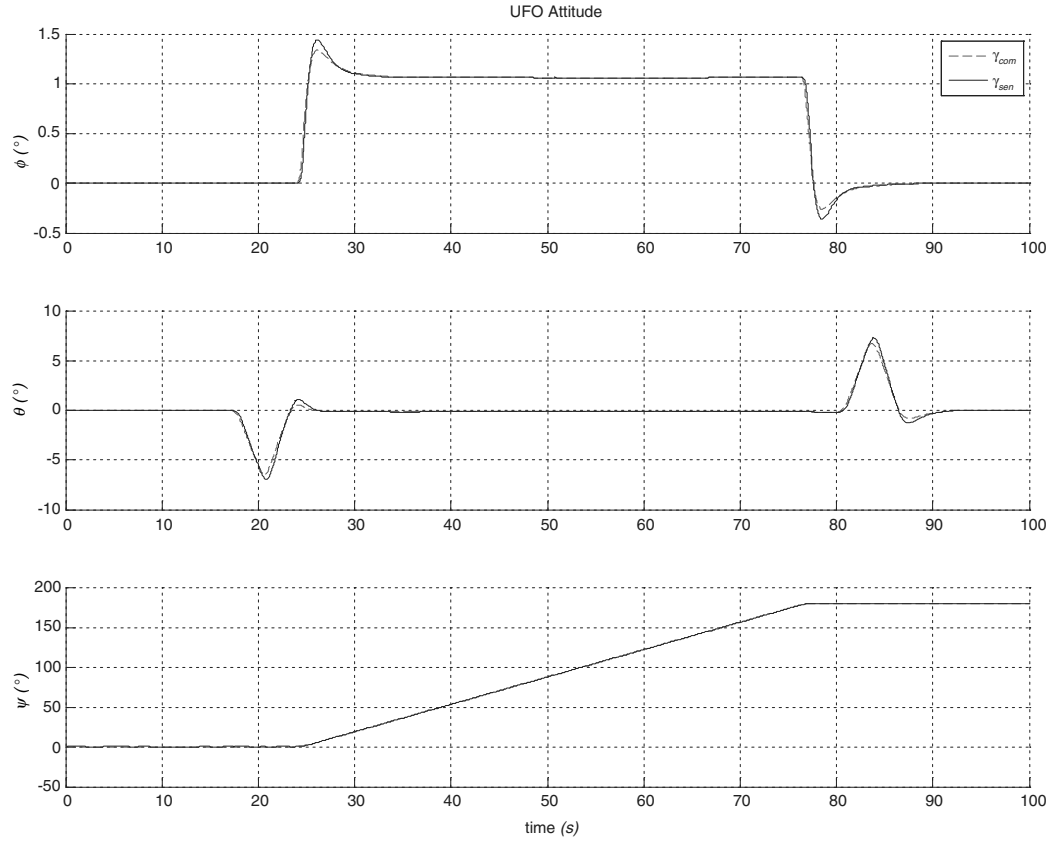

Fig. 9 Euler angle response of command profile tracking.

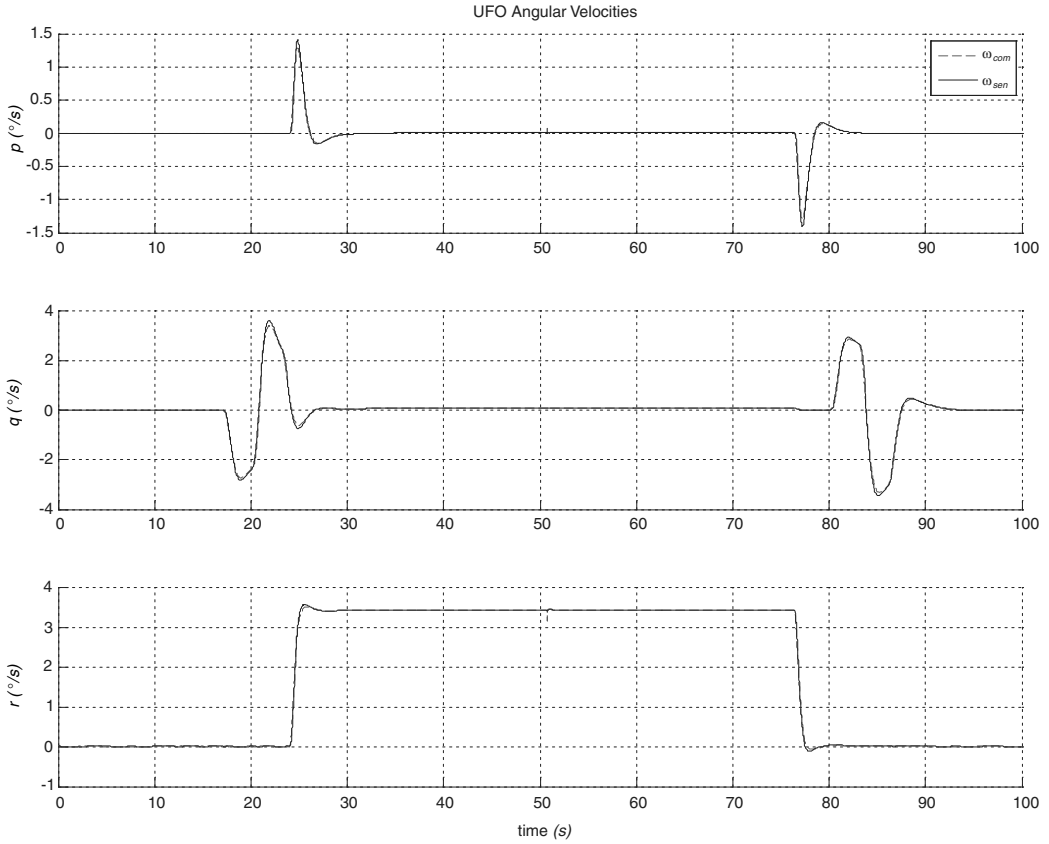

Fig. 10 Angular velocity response of command profile tracking.

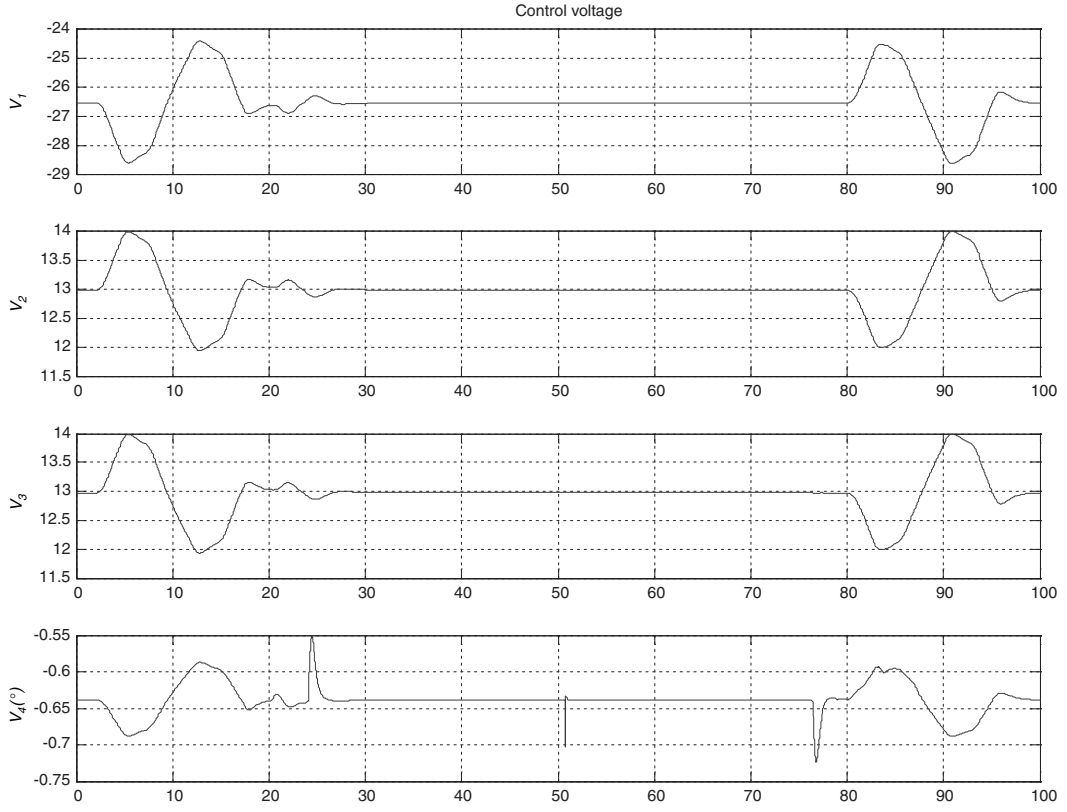

Fig. 11 Actuator input for command profile tracking.

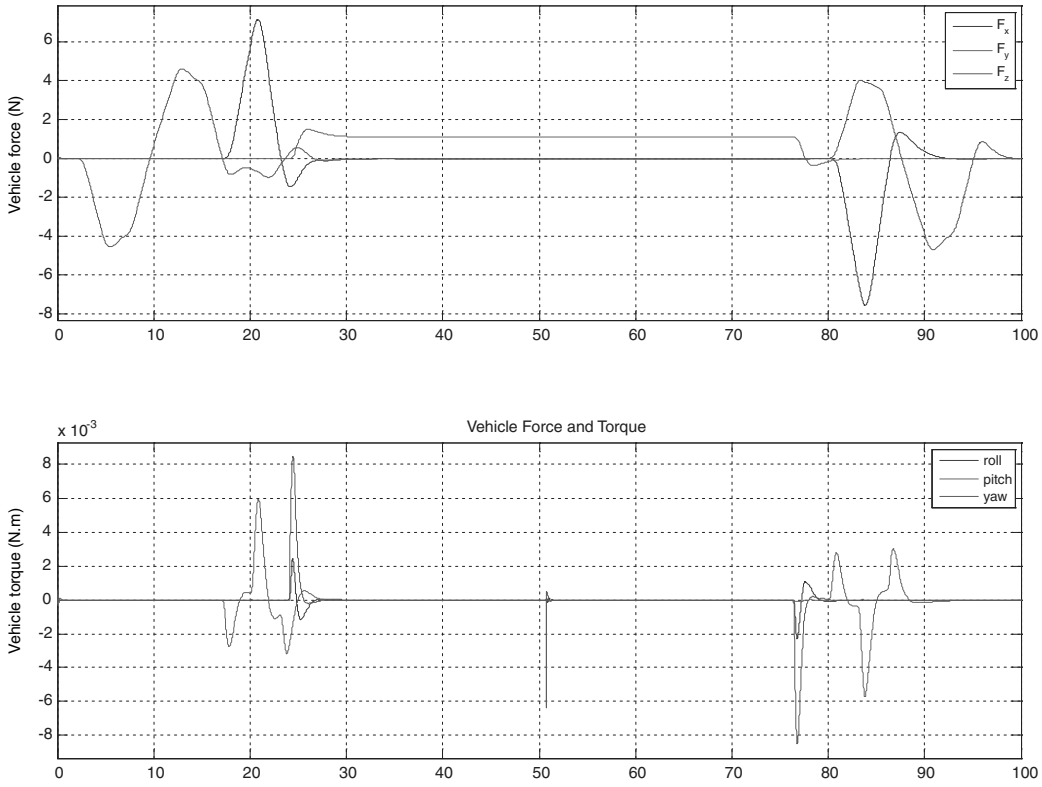

Fig. 12 Vehicle force and torque for command profile tracking.

It is noted that the front motor voltage V_1 is roughly twice that of the rear motors. This can be corrected by adjusting the c.g. location toward the rear of the vehicle. The total forces and torque on the vehicle are plotted in Fig. 12. Overall, the simulation verifies the four-loop 6DOF TLC design.

Case 2: To assess the controller's ability in handling windy and turbulent flight conditions, we tested the nominal design with torque disturbances applied in the roll, pitch, and yaw channels at 30, 40, and 50 s and force disturbances in the body x, y, z directions at 60, 70, and 80 s, respectively, during flight. The torque disturbances are

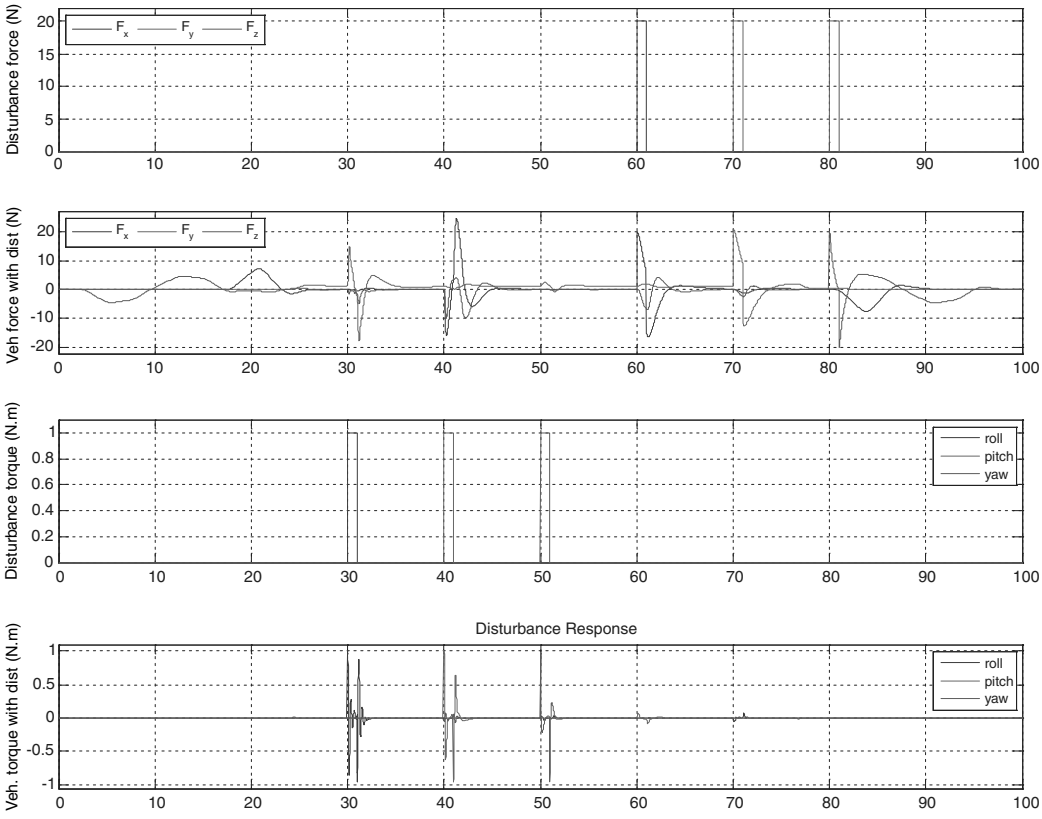

Fig. 13 Force and torque disturbance profile and response.

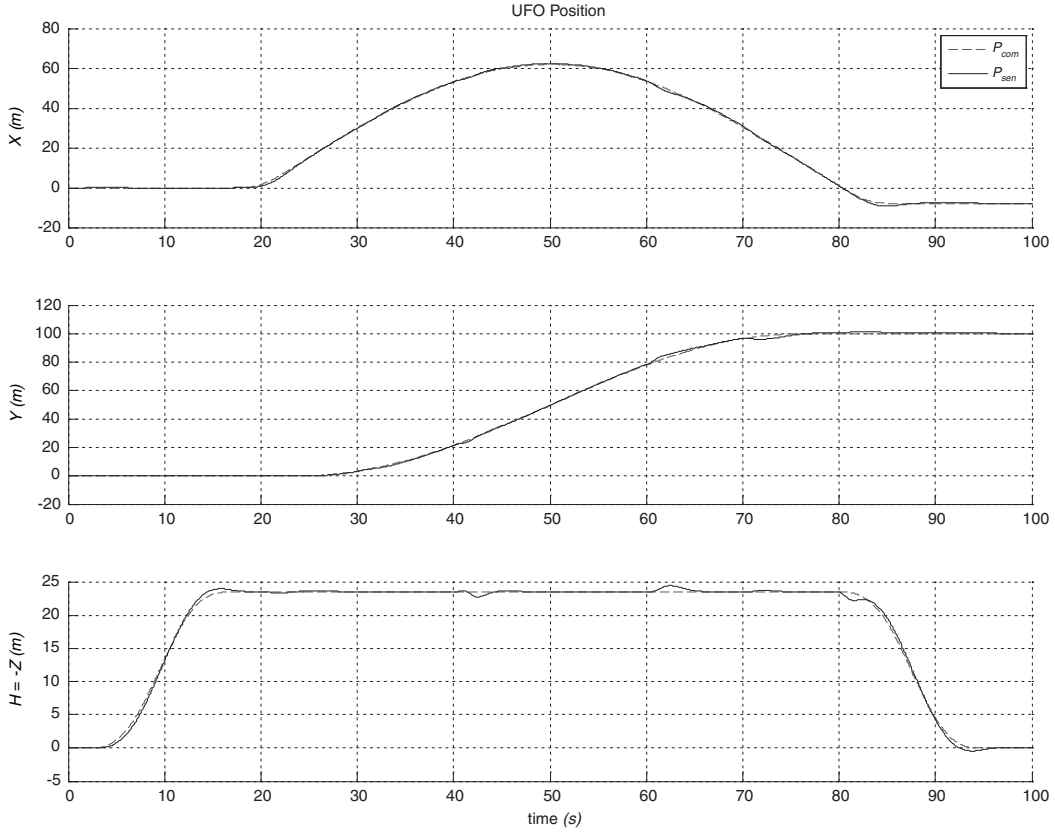

Fig. 14 Position response of command profile tracking with torque disturbance.

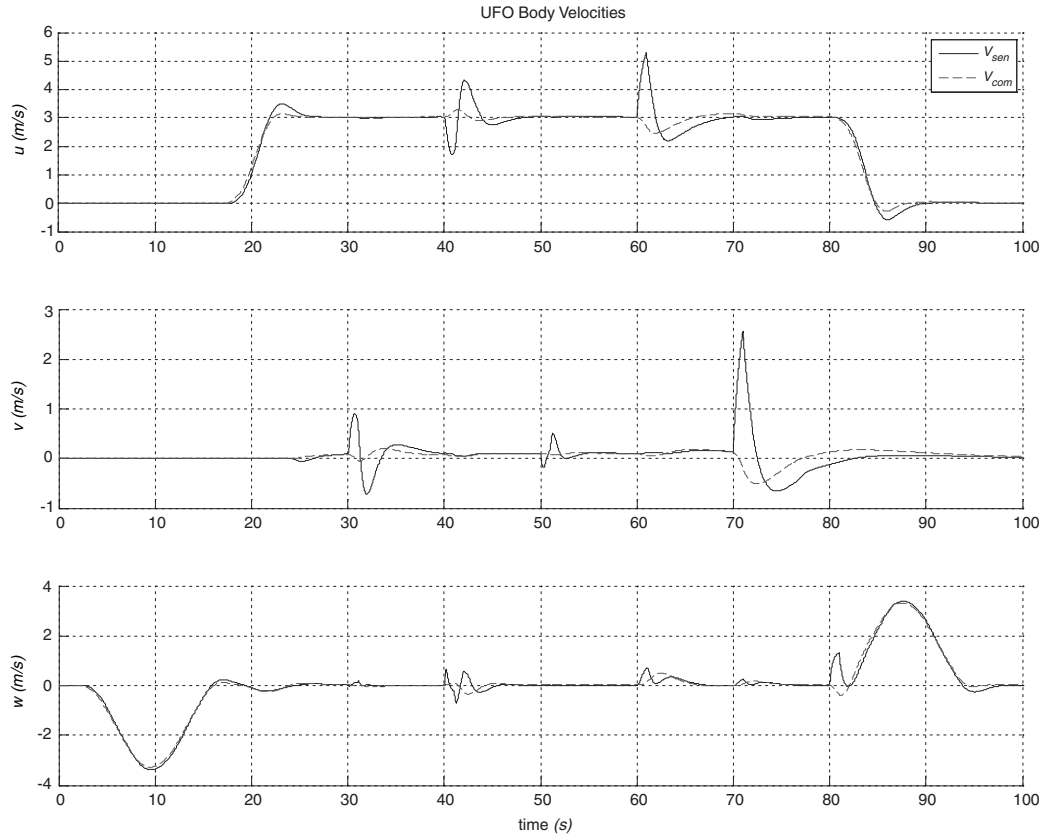

Fig. 15 Velocity response of command profile tracking with torque disturbance.

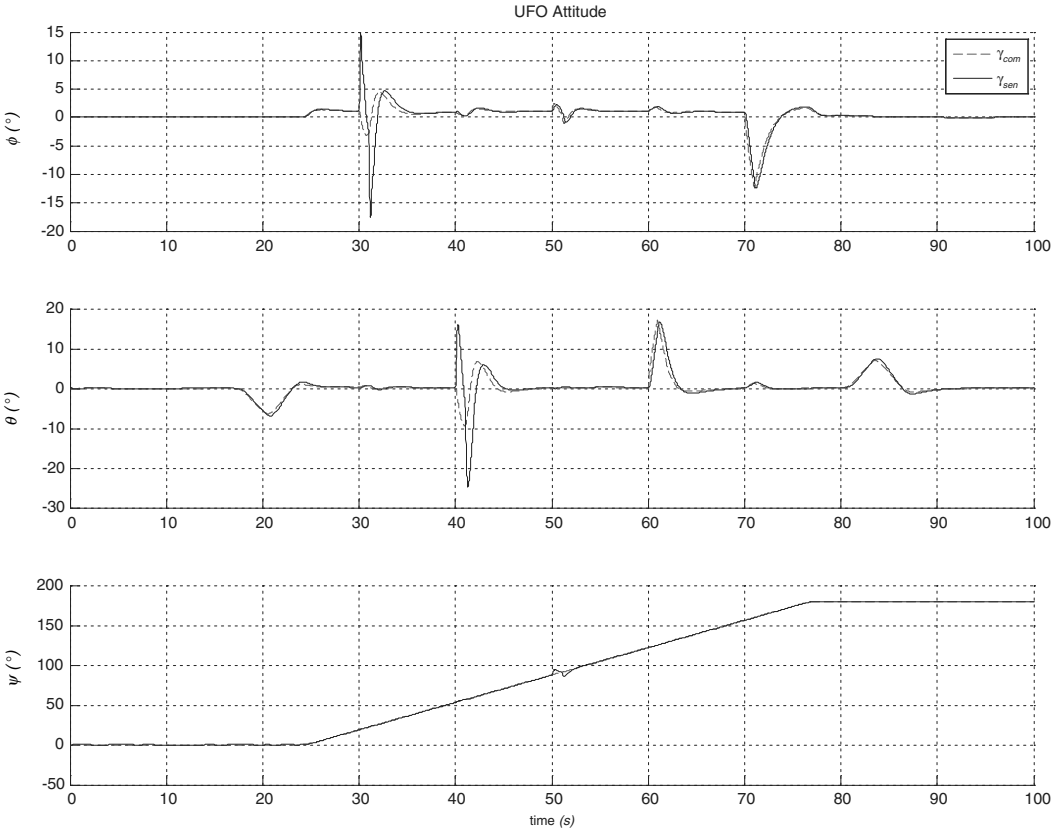

Fig. 16 Euler angle response of command profile tracking with torque disturbance.

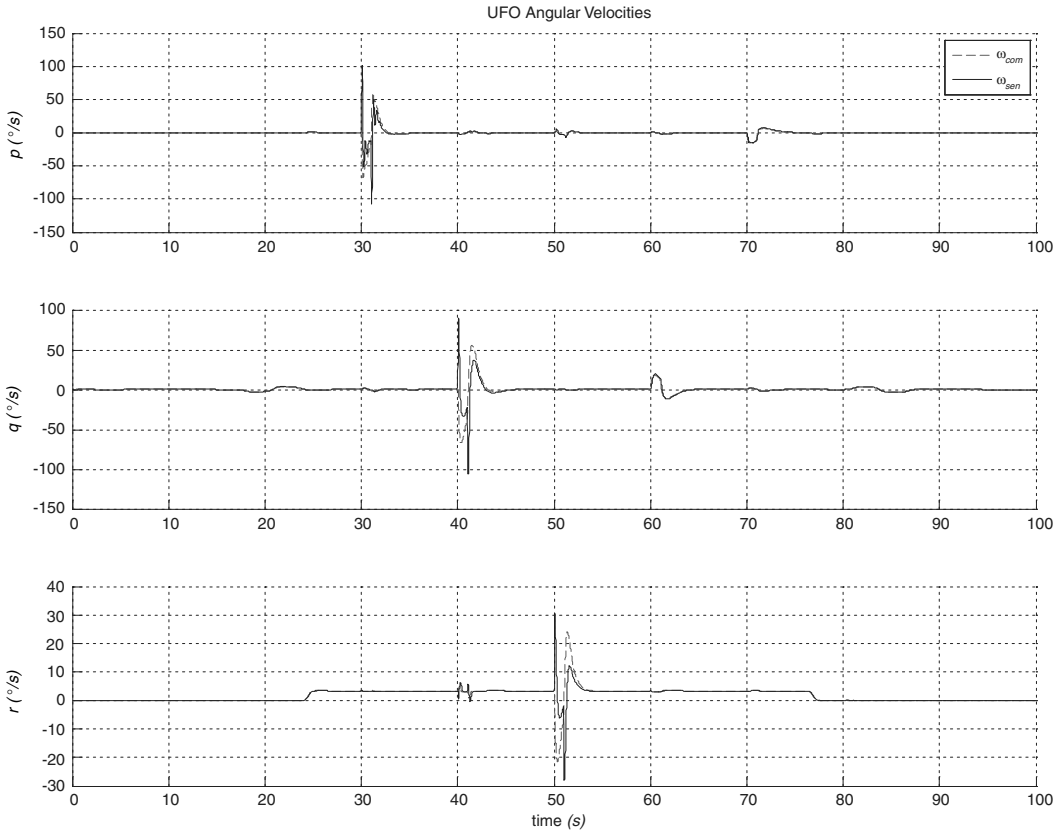

Fig. 17 Angular velocity response of command profile tracking with torque disturbance.

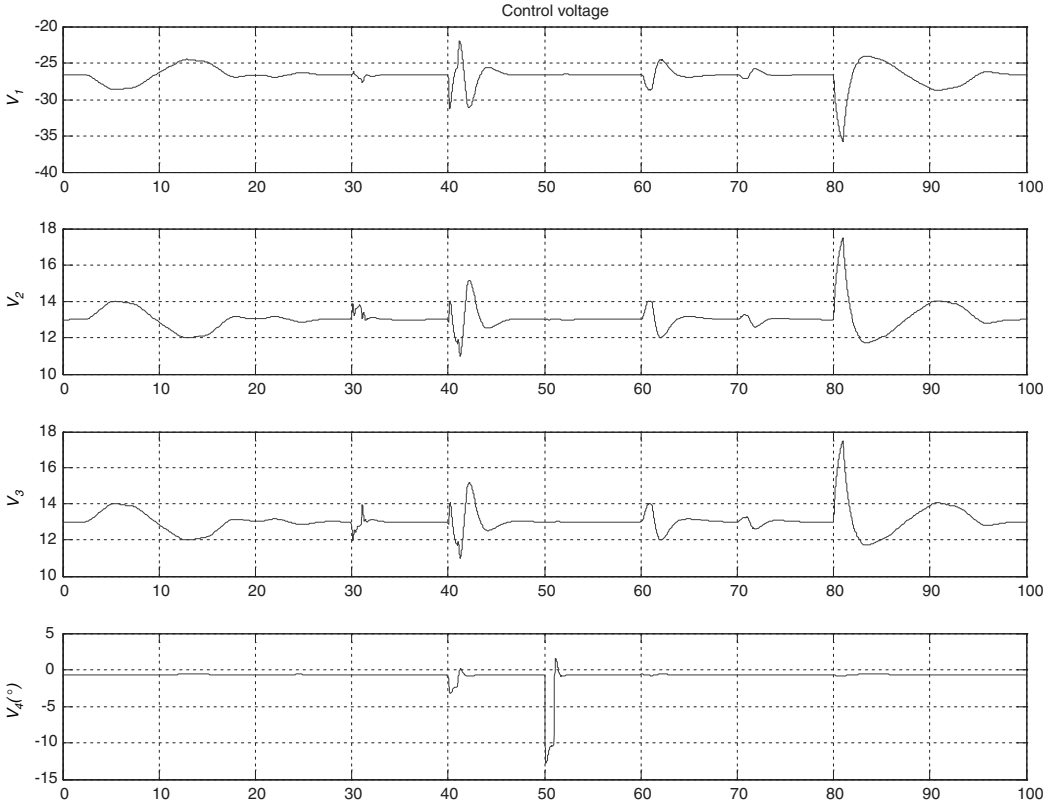

Fig. 18 Actuator input for command profile tracking with torque disturbance.

pulses of 1 s in duration with magnitude 1 Nm for all axes, and the force disturbances are pulses of 1 s in duration with magnitude 20 N in all directions, as shown in Fig. 13. Compared to Fig. 12, it is seen that the magnitude of the disturbance torque is more than 100 times the peak operating torque, and the disturbance force magnitude is 3 times the peak operating force in the x direction, 20 times in the y direction, and 5 times in the z direction. The disturbance force is one-third the vehicle weight and, using the current (very conservative)

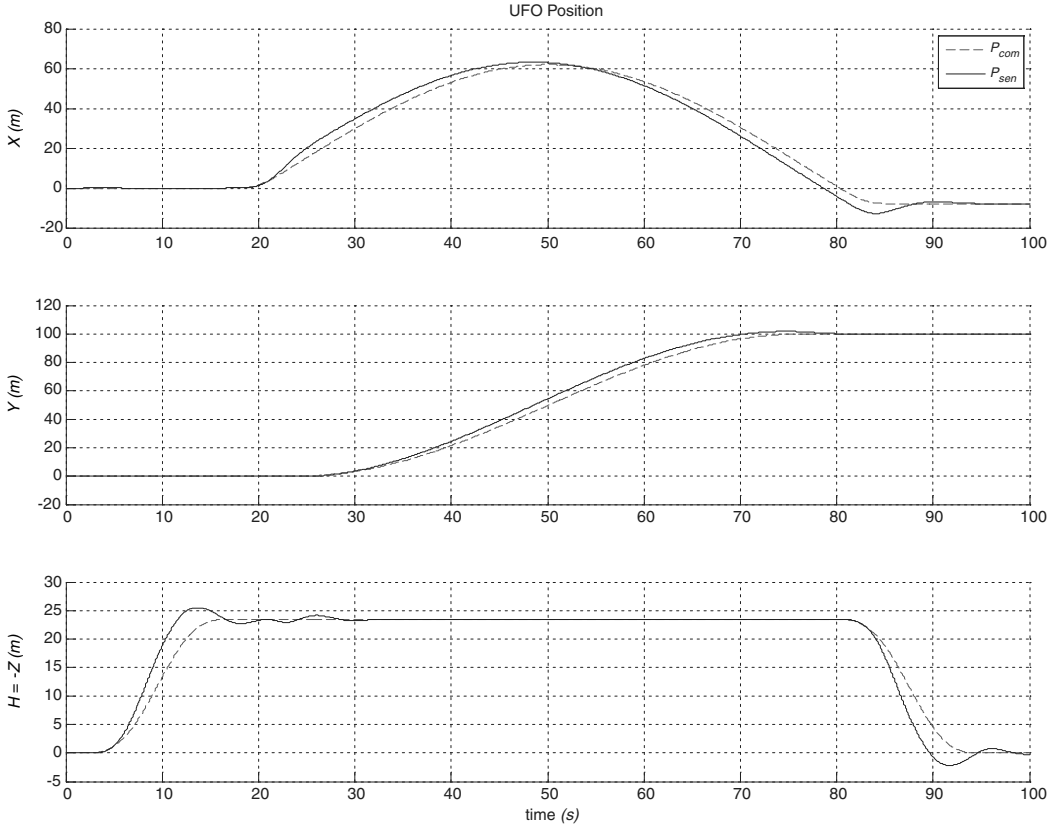

Fig. 19 Position response of command profile tracking with loop delay.

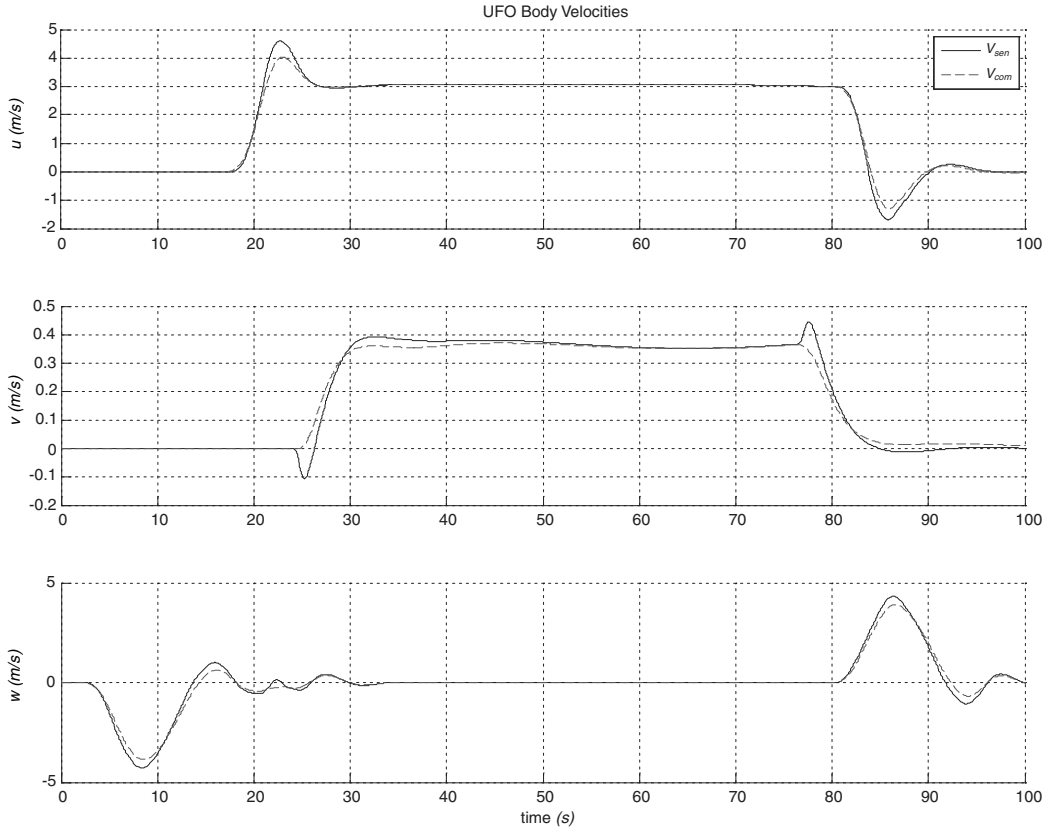

Fig. 20 Velocity response of command profile tracking with loop delay.

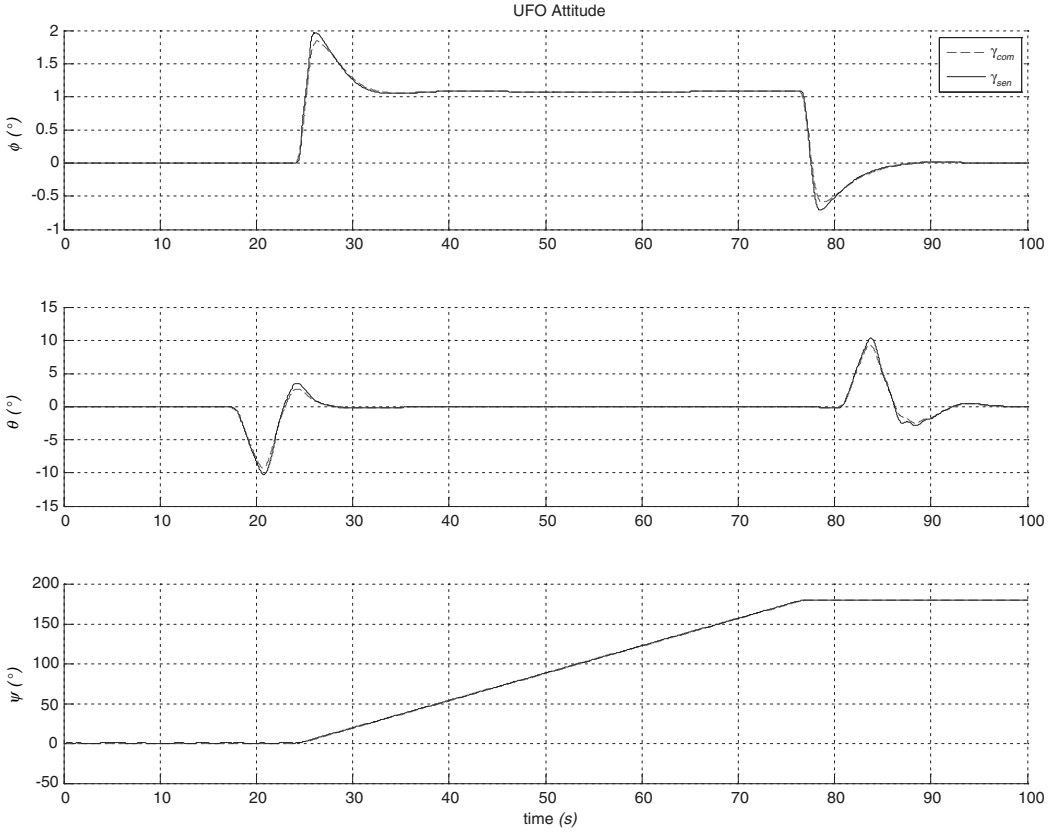

Fig. 21 Euler angle response of command profile tracking with loop delay.

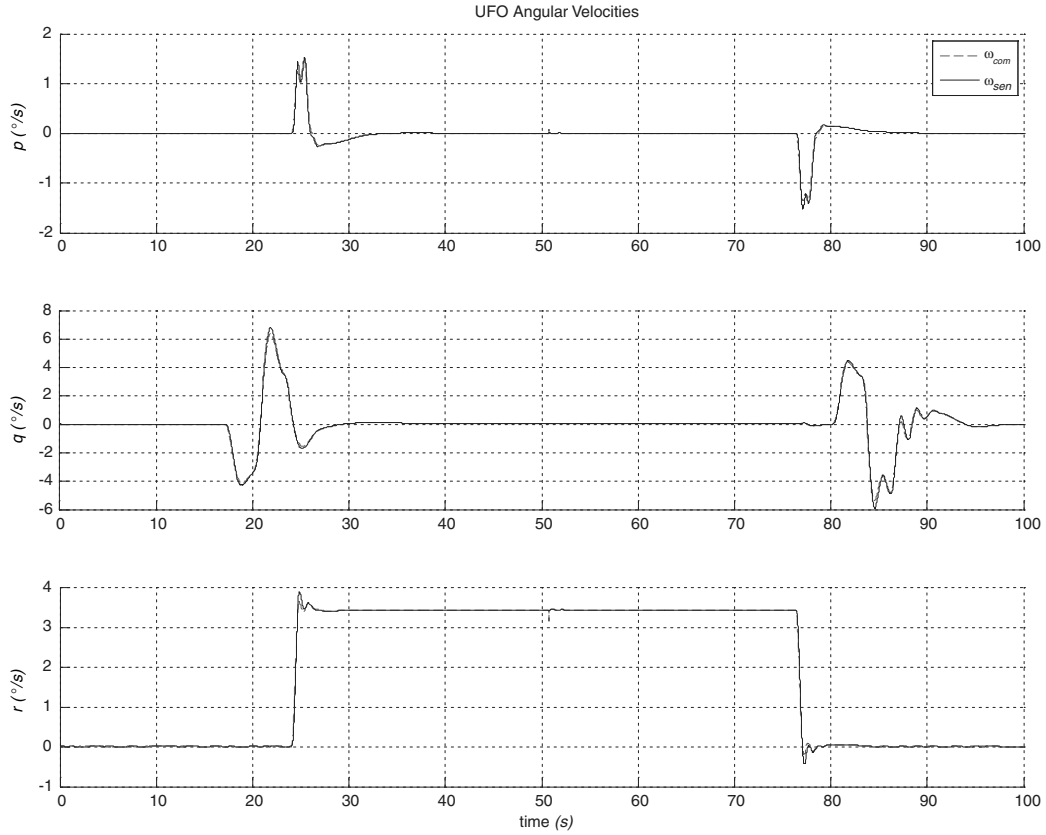

Fig. 22 Angular velocity response of command profile tracking with loop delay.

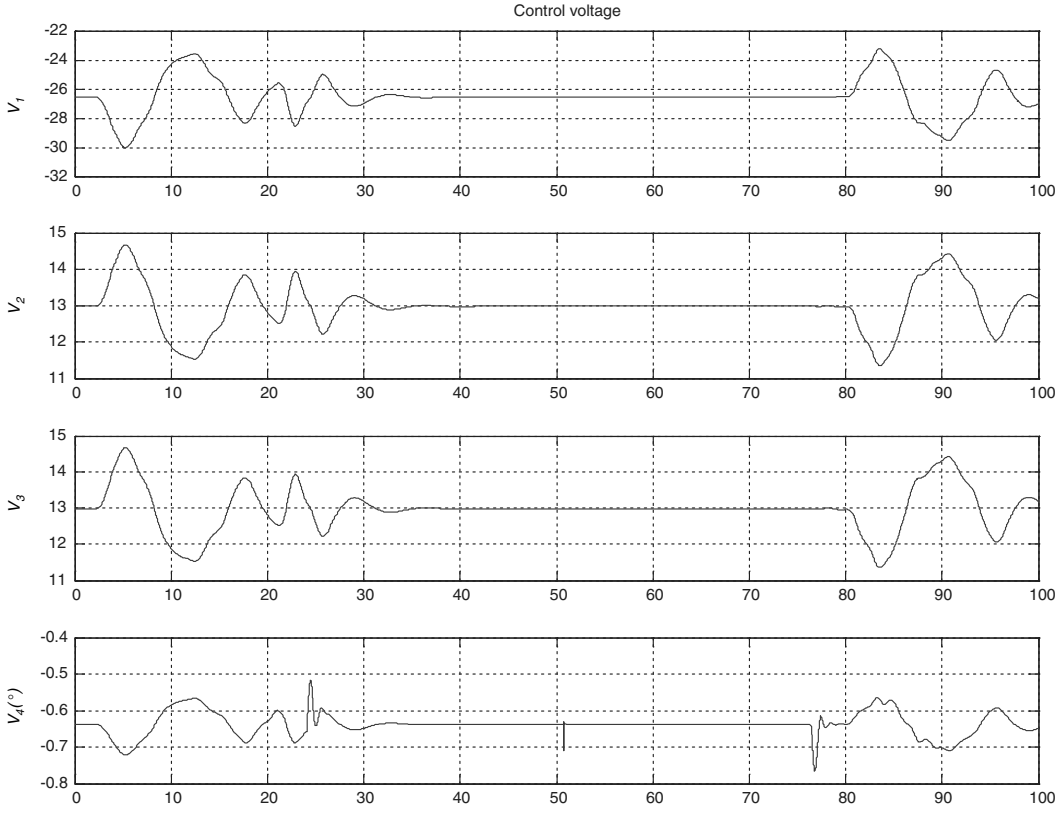

Fig. 23 Actuator input for command profile tracking with loop delay.

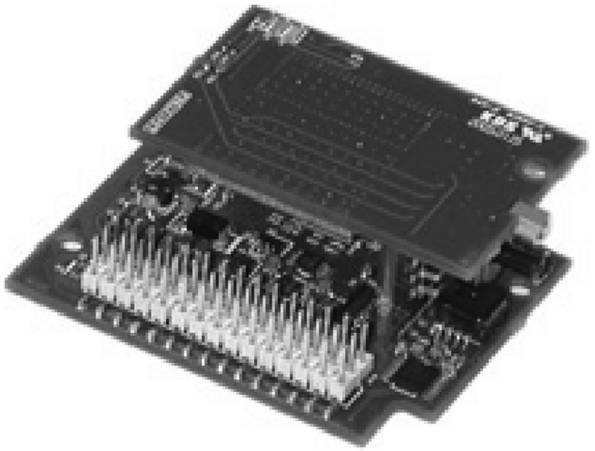

Fig. 24 Crossbow MNAV.

drag model, it would amount to some 60 kt wind. Although the magnitude of the torque disturbances are unrealistically excessive, the TLC controller handles them well. Figure 13 shows the disturbance force and torque profile and the total force and torque applied to the vehicle. It is seen that the controller generated force and torque promptly cancel the disturbance, thereby minimizing their effects. The trajectory tracking and actuator command performance plots are shown in Figs. 14–18. There are no noticeable effects of the disturbance in position tracking, and the actuator commands are all within limits.

Case 3: In this case, a time delay was introduced in each loop, one at a time, to assess its robustness to singular perturbations. The delay was incremented by a small amount until the loop lost stability or the performance became unacceptable. The largest delays each loop could accommodate were as follows: position loop, 2.5 s at 0.1 s increment; velocity loop, 0.6 s at 0.01 s increment; Euler angle loop, 0.19 s at 0.01 s increment; and body rate loop, 0.019 s at 0.001 s increment. These delay margins should be adequate for accommodating parasitic dynamics such as actuator lag, sensor delay, and sampled data implementation. Figures 19–23 show the tracking performance and actuator commands for the nominal design with loop delays of 1.5 s in the position loop, 0.5 s in the velocity loop, 0.15 s in the Euler angle loop, and 0.015 s in the angular rate loop. The tracking errors are somewhat larger than the nominal case, but there is no other noticeable degradation in performance. The delay margin can be increased at the cost of reduced tracking precision and overshoot by decreasing the closed-loop bandwidth ω_n. As a rule of thumb, when ω_n of one loop is decreased, the ω_n for all its outer loops should be decreased by the same factor. This feature can be implemented in real time using the time-varying PD-eigenvalue synthesis [27] for adaptive tradeoff between performance, robustness, and fault tolerance.

Additional tests on robustness of the controller to parametric modeling errors (regular perturbations) were performed by scaling the moment of inertia parameters used in the controller gain calculations to create a mismatch with the vehicle model. The controller was able to accommodate 0.3 and 1.7 times scaling without showing any noticeable degradation in all tracking loops. Using a trajectory linearization observer and extended Kalman filter for state estimation and sensor noise filtering on the 3DOF attitude controller by hardware-in-loop simulation has been reported in [28]. The results are not reported here for brevity.

VI. Implementation of Navigation System

The 6DOF navigation system aboard the UFO consists of a Crossbow MNAV miniature sensor suite (Fig. 24) along with measurement processing software to estimate the state of the UFO. The MNAV sensor package includes accelerometers (3 axis), gyroscopes (3 axis), magnetometers (3 axis), a dynamic pressure sensor for airspeed measurements, a static pressure sensor for altitude measurements, and a GPS receiver. Inertial data output rates from the MNAV are capable of reaching 100 Hz at a baud rate of 57600 bps, with the GPS data output at 4 Hz when adequate satellites are visible. These sampling rates are adequate for the nominal design of the 6DOF TLC flight controller.

The current processing software uses the accelerometers and gyroscopes to create an attitude and heading reference system (AHRS) for 3DOF controls. The GPS unit has also been through initial testing and provides the potential to improve long-term stability in the AHRS, which the low-cost gyroscopes and accelerometers lack.

For the final 6DOF setup, all sensors equipped by the MNAV will be used to provide information for calculation of an optimal navigation solution. This solution will likely involve the use of a Kalman filter for sensor fusion. Additionally, the low-rate GPS measurements can be used to estimate and remove biases found on the inertial sensors. With these biases removed from measurements, lower long-term drifts in state estimates will be produced, thus allowing for longer system stability in the event of loss of GPS lock.

VII. Conclusions

The main results of this paper are the 6DOF TLC flight controller design and simulation testing for the tripropeller VTOL UAV. It is the first time that TLC is applied to 6DOF flight control, and the performance and robustness of the designed controller without any tuning are satisfactory. Future work includes implementing the 6DOF controller presented herein integrated with the 6DOF navigation system on the OU UFO shown in Fig. 1a for 6DOF hardware-in-loop testing and flight testing. Fine tuning of the controller parameters will be needed to account for actuator dynamics, sampling delay, and modeling errors, such as propeller thrust change due to vertical and forward velocity of the vehicle. With the use of inertial sensors, nonlinear observers (estimators), such as the extended Kalman filter, trajectory linearization observer [28], etc., will be implemented to estimate position and attitude from sensed body velocity and angular velocity.

Appendix

$$I^p_{pq} = I_{xz}(I_{yy} - I_{zz} - I_{xx})D \qquad I^r_{qr} = -I^p_{pq}$$

$$I^p_{qr} = (I^2_{zz} - I_{yy}I_{zz} - I^2_{xx})D \qquad I^q_{pp} = -I_{xz}/I_{yy}$$

$$I^q_{rr} = -I^q_{pp} \qquad I^q_{pr} = (I_{zz} - I_{xx})/I_{yy}$$

$$I^r_{pq} = (I_{xx}I_{yy} - I^2_{xz} - I^2_{xx})D \qquad g^p_l = -I_{zz}D$$

$$g^p_n = -I_{xz}D \qquad g^r_l = g^p_n \qquad g^q_m = 1/I_{yy}$$

$$g^r_n = -I_{xx}D \qquad D = 1/(I^2_{xz} - I_{xx}I_{zz})$$

Acknowledgments

The authors wish to acknowledge financial support from the Ohio University 1804 grant, and the following undergraduate students of the School of Electrical Engineering and Computer Science, Russ College of Engineering and Technology, Ohio University, who have participated in the research and development of the Ohio University unique flying object vehicle and guidance, navigation, and control system presented in the paper (in alphabetical order): Najeeb Alhashim, Joseph Althaus, Tim Anderson, Matthew Bauder, Nathan Daniher, Vaibhav Dhawan, Christopher Engel, Rob Hersh, Tyler McCoy, Matthew Metz, Nathan Miller, Anthony Ricelli, Mike Rist, and Ryan Roby. The authors sincerely thank the reviewers for their careful reading of the original and revised manuscripts and their valuable constructive comments.

References

[1] Schultz, J., *Winds of Change: Expanding the Frontiers of Flight, Langley Research Center 75 Years of Accomplishments, 1917–1992*, U.S. Government Printing Office, Washington, D.C., 1992, pp. 83–84.

[2] Prime, Z., Sherwood, J., Smith, M., and Stabile, A., "Remote Control (RC) Vertical Take-Off and Landing (VTOL) Model Aircraft," Level IV Honours Project Final Rept., School of Mechanical Engineering, Univ. of Adelaide, Adelaide, Australia, Oct. 2005.

[3] Salazar-Cruz, S., and Lozano, R., "Stabilization and Nonlinear Control for a Novel Trirotor Mini-Aircraft," *Proceedings of the 2005 IEEE International Conference on Robotics and Automation*, Inst. of Electrical and Electronics Engineers, New York, April 2005, pp. 2612–2617.

[4] Salazar-Cruz, S., Kendoul, F., Lozano, R., and Fantoni, I., "Real-Time Control of a Small-Scale Helicopter Having Three Rotors," *Proceedings of the 2006 IEEE International Conference on Intelligent Robots and Systems*, Inst. of Electrical and Electronics Engineers, New York, 2006, pp. 2924–2929.

[5] Hoffman, G., Rajnarayan, D. G., Waslander, S. L., Dostal, D., Jang, J. S., and Tomlin, C. J., "Stanford Testbed of Autonomous Rotorcraft for Multi Agent Control (STARMAC)," *Proceedings of the 23rd Digital Avionics Systems Conference*, Vol. 2, Stanford Univ., Stanford, CA, Oct. 2004, pp. 12.E.4–121-10.

[6] Weil, P., and Rouillon-Couture, N., Rapport d'activit'e du LIPSI, 2002-2005, Laboratoire en ing'enierie des processus et des services industriels, Ecole Sup'erieure des Technologies Industrielles Avanc'ees, Bayonne, France, 2005, pp. 47–52.

[7] Bouabdallah, S., and Siegwart, R. "Backstepping and Sliding-Mode Techniques Applied to an Indoor Micro Quadrotor," *Proceedings of the 2005 IEEE International Conference on Robotics and Automation*, Inst. of Electrical and Electronics Engineers, New York, April 2005, pp. 2247–2252.

[8] Nice, E. B., "Design of a Four-Rotor Hovering Vehicle," M.S. Thesis, Cornell Univ., Ithica, NY, 2004.

[9] Çamlýca, B., *Demonstration of a Stabilized Hovering Platform for Undergraduate Laboratory*, M.S. Thesis, Middle East Technical Univ., Ankara, Turkey, Dec. 2004.

[10] Sassen, S., and Uhleman, P., *Quattrocopter: A Unique Micro-Aerial Vehicle*, European Aeronautic Defense and Space Company Corporate Research Center, Munich, Nov. 2003.

[11] Guenard, N., Hamel, T., and Moreau, V., "Dynamic Modeling and Intuitive Control Strategy for an X4-Flyer," *Proceedings of the 2005 International Conference on Control and Automation*, Vol. 1, Inst. of Electrical and Electronics Engineers, New York, June 2005, pp. 141–146.

[12] Pounds, P., Mahony, R., Hynes, P., and Roberts, J., "Design of a Four-Rotor Aerial Robot," *Proceedings of 2002 Australasian Conference on Robotics and Automation*, Australian Robotics and Automation Association, Sydney, Australia, Nov. 2002, pp. 145–150.

[13] Hamel, T., Mahony, R., Lozano, R., and Ostowski, J., "Dynamic Modeling and Configuration Stabilization for an X4-Flyer," *Proceedings of the IFAC Symposium*, Vol. 15, Pt. 1, International Federation of Automatic Control, 2002.

[14] Waslander, S. L., Hoffmann, G. M., Jang, J. S., and Tomlin, C. J., "Multi-Agent Quadrotor Testbed Control Design: Integral Sliding Mode vs. Reinforcement Learning," *Proceedings of IEEE/RSJ International Conference on Intelligent Robots and Systems*, Inst. of Electrical and Electronics Engineers, New York, Aug. 2005, pp. 3712–3717.

[15] Wu, X., Liu, Y., and Zhu, J. J., "Design and Real-Time Testing of a Trajectory Linearization Flight Controller for the Quanser UFO," *Proceedings of American Control Conference*, American Automatic Control Council, Evanston, IL, 2003, pp. 3931–3938.

[16] Wu, X., and Zhu, J. J., "A Nonlinear Flight Controller Design for a UFO by Trajectory Linearization Method Part I: Modeling," *Proceedings of the Thirty-fourth Southeastern Symposium on System Theory*, Inst. of Electrical and Electronics Engineers, New York, 2002, pp. 97–102.

[17] Wu, X., and Zhu, J. J., "A Nonlinear Flight Controller Design for a UFO by Trajectory Linearization Method Part II: Controller Design," *Proceedings of the Thirty-fourth Southeastern Symposium on System Theory*, Inst. of Electrical and Electronics Engineers, New York, 2002, pp. 103–107.

[18] Mickle, M. C., Huang, R., and Zhu, J. J., "Unstable, Nonminimum Phase, Nonlinear Tracking by Trajectory Linearization Control," *Proceedings of IEEE Conference on Control Applications*, Inst. of Electrical and Electronics Engineers, New York, 2004, pp. 812–818.

[19] Zhu, J., "PD-Spectral Theory for Multivariable Linear Time-Varying Systems," *Proceedings, 36th IEEE Conference on Decision and Control*, Inst. of Electrical and Electronics Engineers, New York, Dec. 1997, pp. 3908–3913.

[20] Liu, Y., and Zhu, J. J., "Regular Perturbation Analysis for Trajectory Linearization Control," *Proceedings of the 2007 American Control Conference*, American Automatic Control Council, Evanston, IL, July 2007, pp. 3053–3058.

[21] Liu, Y., and Zhu, J. J., "Singular Perturbation Analysis for Trajectory Linearization Control," *Proceedings of the 2007 American Control Conference*, American Automatic Control Council, Evanston, IL, July 2007, pp. 3047–3052.

[22] Bevacqua, T., Best, E., Huizenga, A., Coope, D., and Zhu, J., "Improved Trajectory Linearization Flight Controller for Reusable Launch Vehicles," *AIAA Proceedings of the 42nd Aerospace Sciences Meeting and Exhibit Conference*, AIAA Paper 2004-875, 2004.

[23] Zhu, J.; Banker, B. D., and Hall, C. E., "X-33 Ascent Flight Controller Design by Trajectory Linearization: A Singular Perturbational Approach," AIAA Paper 2000-4159, Aug. 2000.

[24] Zhu, J. J., and Huizenga, A. B., "A Type Two Trajectory Linearization Controller for a Reusable Launch Vehicle: A Singular Perturbation Approach," *Collection of Technical Papers: AIAA Atmospheric Flight Mechanics Conference*, Vol. 2, AIAA, Reston, VA, 2004, pp. 1121–1137.

[25] Liu, Y., Williams R., II, Zhu, J. J., and Wu, J., "Omni-Directional Mobile Robot Controller Based on Trajectory Linearization," *Robotics and Autonomous Systems*, Vol. 56, No. 5, 2008, pp. 461–479. doi:10.1016/j.robot.2007.08.007

[26] McRuer, D., Ashkenas, I., and Graham, D., *Aircraft Dynamics and Automatic Control*, Princeton Univ. Press, Princeton, NJ, 1972, pp. 227–233.

[27] Zhu, J., Lawrence, D. A., Fisher, J., Shtessel, Y., Hodel, A. S., and Lu, P., "Direct Fault Tolerant RLV Attitude Control: A Singular Perturbation Approach," AIAA Paper 2002-4778, Aug. 2002.

[28] Huang, R., and Zhu, J. J., "MIMO High Gain Trajectory Linearization Observer Design," *Proceedings, 2007 American Control Conference*, American Automatic Control Council, Evanston, IL, July 2007, pp. 248–253.